12-2020

Biometric Face Skintone Data Augmentation Using A Generative Adversarial Network

Rosalin Dash

Biometric Face Skintone Data Augmentation Using A Generative Adversarial Network

by
Rosalin Dash

Bachelor Of Technology
Electronics and Communication Engineering
Gandhi Institute of Engineering and Technology
2012

A thesis
submitted to the College of Engineering and Science at
Florida Institute of Technology
in partial fulfillment of the requirements
for the degree of

Master of Science
in
Computer Science

Melbourne, Florida
December, 2020

We, the undersigned committee, hereby approve the attached thesis.

Biometric Face Skintone Data Augmentation Using A Generative Adversarial Network

by
Rosalin Dash

Michael King, Ph.D.
Major Advisor
Associate Professor
Computer Engineering and Sciences

Kevin Bowyer, Ph.D.
Committee Member
Honorary Professor
Biomedical Technologies

Munevver Mine Subasi, Ph.D.
Outside Committee Member
Associate Professor and Department Head
Mathematical Sciences

Philip Bernhard, Ph.D.
Associate Professor and Department Head
Associate Professor
Computer Engineering and Sciences

Abstract

Title:

Biometric Face Skintone Data Augmentation Using A Generative Adversarial Network

Author:

Rosalin Dash

Thesis Advisor:

Michael King, Ph.D.

Researchers seek methods to increase the accuracy and efficiency in identifying an individual using facial biometric systems. Factors like skin color, which may affect the accuracy of facial recognition, need to be investigated further. To analyze the impact of race with respect to skin color of face on biometric systems, we focused on generating a dataset with uniformly distributed images of different skin tones while preserving identities. Deep learning neural network architectures like the generative adversarial network (GAN) focus on modifying only certain features of the face like the color of the skin. In our experimental approach, we implemented a cycle GAN to synthesize multiple images of individuals with varying color of their skin based on the Fitzpatrick scale. The Fitzpatrick scale defines six levels of skin tone, with FP-1 representing a lighter and FP-6 a darker shade of color. The resulting GAN receives an image of a person with a skin tone labeled FP-1 as its input and synthesizes five additional images to show what that person would look like with skin-tone ratings of FP-2 to FP-6. A GAN was trained to receive an image of a person with a skin-tone rating of FP-6 and subsequently to produce images corresponding to skin-tone ratings of FP-5 to FP-1. The Arcface matcher was used to measure the similarity between the original images of a person and those produced by the GAN. The results of the analysis indicate a drop in the similarity scores when skin tones change from light to dark and vice versa. In future work, we intend to train a facial recognition algorithm to evaluate the impact of bias relative to skin tone with uniformly generated improved version of skin color images of the same individual.

Table of Contents

List of Figures

List of Tables

Acknowledgments

I take this opportunity to express my profound gratitude and deep regard to my advisor and mentor Dr. Michael King for his guidance, regular monitoring, and constant encouragement throughout the course of this thesis.

I also take this opportunity to express a deep sense of gratitude to my parents Dr. Rama Chandra Dash and Dr. Sabitri Satapathy; I owe thanks to a very special person, my late husband Gopal Satpathy, for always having the confidence in me which motivated me to aspire more in life, along with my brother and sisters, for being there and supporting me in every decision of life.

I am obliged to identity lab team members and my committee members for the esteemed information provided by them in their respective fields. I am grateful for their cooperation during the period of my assignment.

Lastly, I would like to thank Manas Bhattacharya and Tapas Joshi for their assistance in proofreading the thesis document and have given it a dynamic way by their information and feedback. I am glad to thank my friends Ravi Pandhi and Adolf D'Costa for being a constant support during this two-year journey.

Chapter 1

Introduction

Rapid advances in science include the exploration of biometric technology for identification purposes. Because humans are complex organisms, establishing identity is essential for recognizing people to understand if they are who they claim to be. Researchers find that developing systems for identifying individuals with different behavioral and physical characteristics is challenging when establishing identity. They invest much time focusing on other aspects of human behavior and physiological factors that affect the performance measurements of biometric systems.

The evolution of the facial recognition systems (FRS) has made its way to many fields covering airports, border security, law enforcement, and even software for banking transactions. Due to the diverse use of FRS, it is essential to identify a person appropriately. A recent study by NIST evaluates the effects of demographics and highlights other soft biometric traits on facial recognition software, such as age and sex [6]. As one of our previous work characterizes the variability of two different cohorts, the African American and the Caucasian, with different threshold accuracy [21], eradication of bias involvement becomes crucial. The necessity of facial recognition algorithms (FRA) to operate at a uniform threshold across cohorts is indispensable. Top performing algorithm identified faces at 99.64% accuracy for true positive or same person comparisons and 99.999% accuracy for false positive or different person comparisons. Another 50 different algorithms benchmarks that identified faces with at least an accuracy of 98.75% for same person comparisons and 99.999% accuracy for different person comparisons [13].

Due to rapid advancement in deep learning technology, a convolutional neural network (CNN), approaches how skin tone can be extracted and classified into three categories: light, medium, and dark [1]. The further classification of skin as cool, warm, and neutral originated from the idea of the skin's undertone, irrespective of tanning effect. As dermatologists classify skin into six Fitzpatrick classes [22]. The CNN approach thus lacks intermediate skin tones. Prior work of understanding the unequal gender classification accuracy for face images; eradicates skin tone as a factor for discrepancy in dark-skinned females [19]. Their approach focus on training and understanding bias by using IBM Watson [20] and other customized neural network with a ResNet-50 [9] architecture. The luminance mode shift and optimal transport procedures are used to analyse the impact of skin tone.

Our experimental approach focuses on establishing the more complex and finer classification schemes by utilizing the widely popular deep learning generative adversarial network (GAN). GAN is a powerful approach to machine learning (ML). At a high level, a GAN is a combination of two neural networks that feed into each other, one producing increasingly accurate data with the other improving the ability to classify such data. The neural network architecture gradually learns the details about the entire dataset and eventually tries to superimpose the training model into the test image. GAN architecture improves neural network ability to learn more about the images that are visually indistinguishable. The GAN generator module helps to generate images close to the train input set, thereby making them difficult to be identified. Thus, benefits of the neural network include the generation of a new dataset from the pre-existing one with different skin types. The newly generated dataset can help eradicate the bias caused in the FRA by uniformly distributing the skin color of an individual and preserving the identity, regardless of the variation in skin tone.

This thesis proposal introduces the GAN approach that considers images manually rated according to the Fitzpatrick Type I (FP-1) category and uses GAN neural network architecture to hallucinate face skin tone and generate the subsequent FP-2 to FP-6 of the same image. Similarly, the GAN analyzes images rated as FP-6 and generates copies that alter the skin tone from FP-1 to FP-5. In the initial approach, we considered performing the experiment using beauty GAN architecture, but due to the lack of clear demarcation in the Fitzpatrick scale images, we modified the approach by changing the architecture to cycle GAN. The generated sample images of both the approaches were observed, and analysis were carried out on the cycle GAN architecture using the Arcface matcher.

Chapter 2

Background

2.1 Biometrics

In the current world of digitization, security can be maintained primarily using either password-based systems or biometric security systems [15]. Password systems are susceptible to hackers, while biometric-based systems are less susceptible to change, and unique to each individual. Biometric is defined as a measurement of certain biological features of a human body [10], which acts as biometric traits for defining a biometric authentication system. These biometric traits can be unique, permanent, and are less susceptible to change because of its existential nature.

2.1.1 Categorization of Biometrics Authentication System

A biometric authentication system is defined as a system that uses certain biometric traits for verification and authentication. The biometric traits defined by these systems can be broadly classified into three major characteristics: the physiological, which deals with the physical existence of human body features like eyes, ears, feet, and fingerprints; the behavioral which is defined by the way humans project themselves or acquires certain behavior over time and the chemical or biological which characterizes the internal biological factors that define the existence of human bodies like DNA, veins, melanin (skin color), etc [27]. Figure 2.1 represents various biometric traits and their categorization on the basis of the above classification technique.

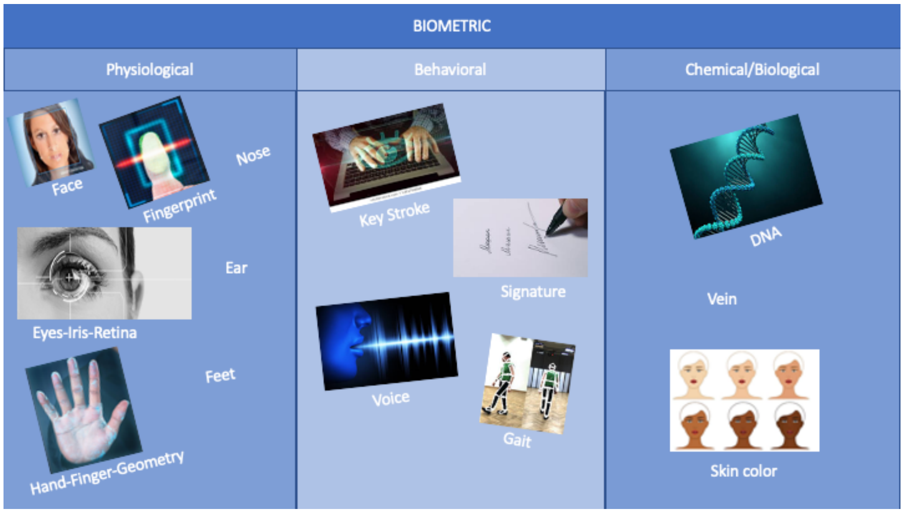

Figure 2.1: Biometric Systems Classification
kulkarni$_2$018, [16], [29], [25], [28], [11],

2.1.2 Applications of Biometrics System

The use of a biometric authentication system has shown constant growth across the globe for myriad reasons but most applications of these systems have three primary purposes i.e verification, identification, and duplicate checking [7]. Looking at the top five uses of these systems worldwide we can define places where these systems are used on a daily basis for more security, and convenience. Biometric system is used to cover airport security, in the identification of passengers for seamless entries, time and attendance of employees in organizations for establishing their identities, law enforcement for verification of an individual against the evidence collected, access control and single sign-on(SSO) for verifying if the individual requesting for access is the same person i.e comparing with “what they are” to “what we know” and “what we have” and bank transaction authentication for verification of the persons identify with the details of its own to grant access to their own accounts [**m2sys_2020**]. We can also use biometric traits for fraud detection and check for the existence of multiple records for social benefit programs.

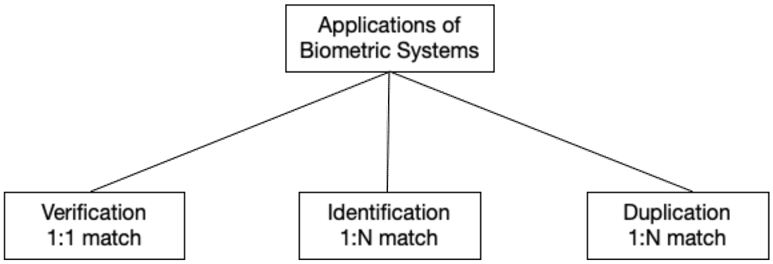

Figure 2.2: Applications of Biometric Systems

Figure 2.2 above classifies the applications of Biometric Systems into three major types. Verification is classified as a 1:1 match, as a single biometric trait is obtained from an individual and is checked one by one to obtain the highest-scoring match where the threshold of the comparison is kept high to know “Are you who you say you are”. On the other hand, identification performs a check on the entire gallery of images in the database to establish “Are you someone who is known to the system”. Duplication is also a kind of identification establishment in the search of finding duplicates of the person in the gallery of a single existence to prevent fraud.

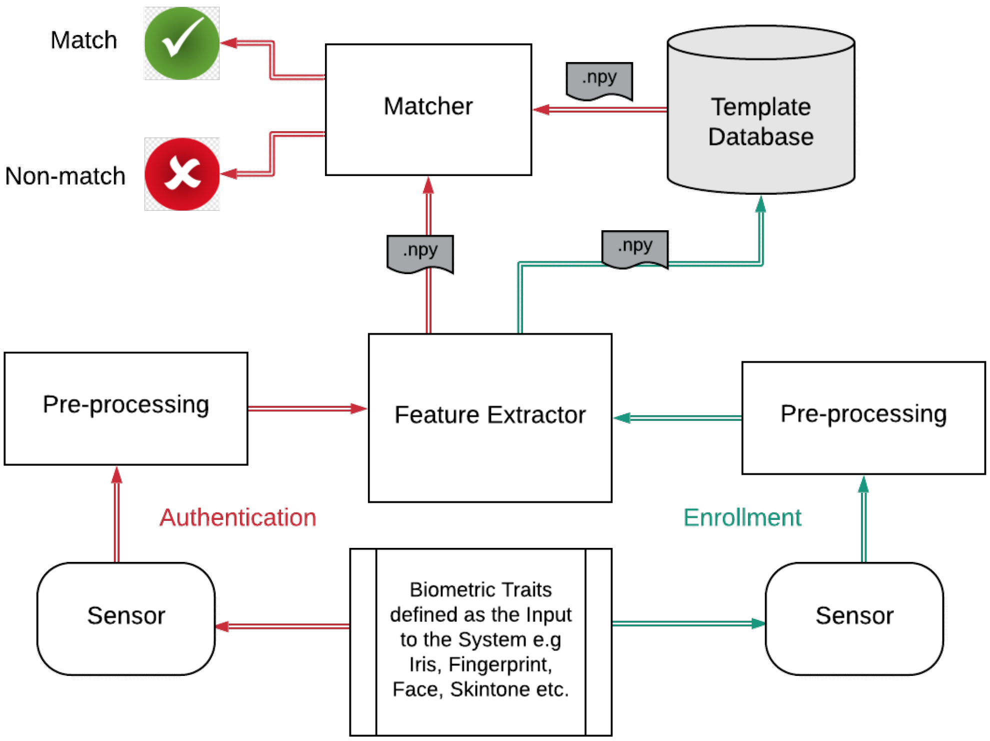

Figure 2.3: Overview of a Biometric Authentication System

2.1.3 Process Involved in Biometric Detail Extraction

To establish a biometric authentication system for verification or identification, the system is categorized into different modules where each module performs a specific set of tasks. Figure 2.3 below represents the block diagram and the flow of a generic biometric system. The various building blocks or modules used to define these systems are sensor module, preprocessing, feature extraction, database, and matcher module. Each module captures and processes details about individual identity. The process of this capture is divided into two categories; enrollment, and recognition [10]. During the enrollment phase, the biometric traits as decided by the design of the system are captured and are stored in the database as templates. During the recognition or authentication phase, the biometric trait is again captured and is compared to the templates already present in the existing database. Once the matcher compares the templates against the existing templates, it either generates a match or a non-match to establish the identity of the individual.

2.1.4 Multimodal Biometric Systems

Multimodal biometric systems capture more than two biometric traits and fuses it into a single template file for matching against the authenticator. The various biometric recognition solutions comparison as stated in 2.1 [26] gives a gist of how the unimodal biometric solution doesn't provide enough level of security which makes them vulnerable for spoofing and hacking attempts.

Table 2.1: Overview of Biometrics Uni-modal Characteristics

Measurement Parameters	**Facial Recognition**	**Iris Scanning**	**Fingerprint Identification**	**Voice Verification**
Accuracy	Medium-low	High	High	Medium
Sensors	Camera	Camera	Scanner	Microphone
Resistance	Lightening, Glasses, hair,motion, age,skin-tone	Lightening, eye movement,lenses	Dryness, dirt,injury, age	Noise, cold
Attack Precautions	Average	Very high	High	Average
Verification Delay	3 seconds	less than 5 seconds	less than 3 seconds	5 seconds

Other reasons for the increasing demands of the multimodal biometric system include strong liveness detection of the individual, option to consider other biometric traits in case of disabilities, inclusion of multi modalities that ensures high accuracy for identification and can neglect the input traits coming from faulty sensors by still maintaining the accuracy [23]. The efficiency of biometric systems is determined using image acquisition errors and the matching errors [30]. Image acquisition error can be further classified into failure-to-acquire (FTA) and failure-to-enroll (FTE); and matching error into false-non-match rates (FNMR) and false match rate (FMR). FNMR is the error caused when a legitimate person is rejected where FMR is due to an imposter gaining access to the system. In the case of a multimodal biometric system, FTA, FTE, and FMR are almost zero leading to open areas for research.

2.1.5 Necessity Of Soft Biometrics

Due to the increased use of multimodal biometrics to enhance security, additional biometric traits called soft biometrics like the gait, gender, periocular, color of the skin, etc improves the overall performance of the system. Soft biometric can also play a significant role in identifying individuals when the primary biometric traits are either corrupted or unavailable. This has proved to be of major importance in identifying subjects for crime scenes by providing extra details about the suspect like tattoos, marks, shoe size, and, the ethnicity of the suspects.

2.2 Deep Learning

Due to the increased need for automation in various industries, artificial intelligence (AI) is often relied upon to assist in making complex decisions. The subset of AI i.e machine learning (ML) helps in identifying and categorizing images over a set of known or unknown images. Deep learning, a fragment of ML, carries out the ML process using neural networks. These networks learn features of the phase of the image by phase in each layer and come to certain probabilistic conclusions of identifying the images. The arrangement of weights and biases of the neural network to achieve the desired outcome is defined as deep learning.

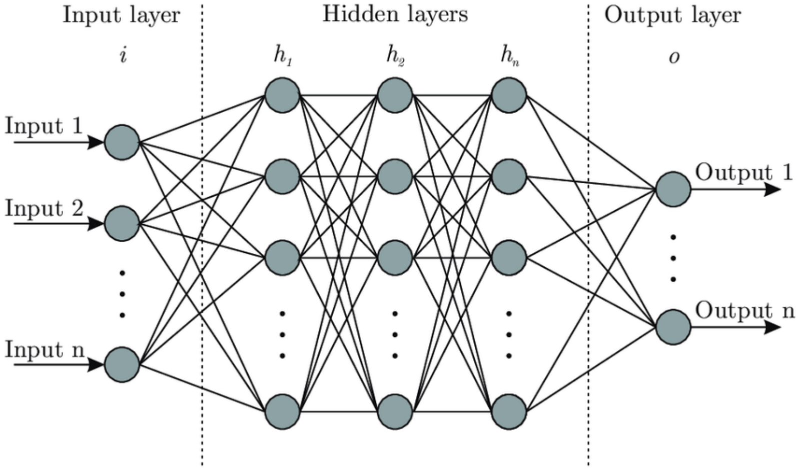

Figure 2.4: Simple Neural Network Architecture
[24]

2.2.1 Application of Neural Network in Image Processing

The biometric traits when captured from the sensors are in the form of images. Image processing helps to extract minute details of these biometric traits and validates the identity of an individual. Figure 2.4 below defines a simple neural network architecture in which the first layer acts as the input layers which reads the image and the hidden layers consecutively filter certain necessary details about the image and pass it onto the next layers. In the last layers, the output layer identifies the probability of the image being identified as a defined category. The adjustment of these weights and biases at each layer of the neural network to improve the efficiency of identification of an image is called image processing. When the same set of identification is done over a similar category of images, neural networks, like the brain, learn a particular pattern of the image and improve its output probability when subject to any random image. As biometric a field of extracting and processing biological traits from the finger, face, and, iris images, images processing, and neural network acts as the backbone for learning features from a source Image.

2.2.2 Generative Adversarial Network

A GAN is a special type of neural network architecture where two neural networks compete with each other to generate the desired output, matching the input dataset of images. The two neural networks fight with each other, a convolutional neural network (CNN) which is termed as a generator, and a classification neural network which is the discriminator. Adversarial refers to the system improving itself by the focus on its own weakness. The output generated by the generator is classified by the discriminator and if the discriminator fails to identify by throwing a probability of 0.5, then the output is really close to the probability distribution of the input dataset. On the other hand, if the discriminator is rightly able to identify the fakeness of the image, then the generator is trained with error thereby adjusting its weight and biases by back-propagation. The adversarial technique helps generate an image as close to the input dataset probability distribution where the discriminator fails to identify.

Figure 2.5 illustrates a GAN architecture with a generator and a discriminator network, and the random noise is the latent space which acts as the source input images to the GAN architecture whose probability distribution should be made

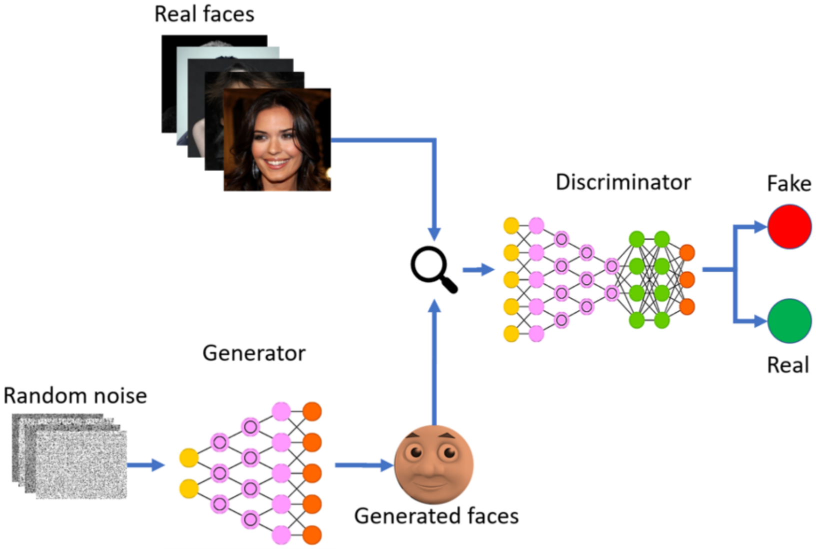

Figure 2.5: Generative Adversarial Network Architecture [14]

similar to that of the real face images thereby trapping the discriminator to wrongly identify the target generated image. The ability of GAN to generate visually realistic images is achieved by training the generator with the gradient of its discriminator model.

2.3 Literature Review

This section of the chapter gives a thorough background of all the related works which are beneficial and motivated me towards the contribution of this thesis work. The Section Beauty GAN, Style GAN below throws light on different GAN architecture and other skin tone related works in the field of neural networks. It also gives certain details about the dermatologist skin classification approach.

2.3.1 Style GAN

A style based generator architecture for GAN talks about a new generator architecture where they have introduced an additional intermediate latent space that uses affine transformation [12], adds gaussian noise, and performs an adaptive instance normalization (AdaIN) to each convolution layer in the introduced generator architecture. This paper gives a detailed analysis of the performance of the new architecture at each introduced step and how it differs from traditional generator architecture. It also offers a new Flickr-Faces-HQ (FFHQ) dataset with 1024*1024 resolution images with more variations with respect to age, ethnicity, image background, and other facial accessories.

2.3.2 Beauty GAN

The beauty GAN paper talks about instance-level facial makeup transfer with deep GAN [17]. Considering source A as a makeup image and source B as the non-makeup image, they have tried to superimpose the makeup source A onto the face in source B without changing the face structure and the texture of the face image. They have tried to achieve the makeup transfer at a domain-level by introducing perpetual loss and cycle consistency loss to maintain the background information of the image. To extract details further at instance-level like extracting color transfer features like eyeliner, lipstick, or foundation they have introduced histogram loss over the particular region of interest. It also introduced a facial makeup dataset comprising no-makeup images and 2719 makeup images.

2.3.3 Exploring Racial Bias within Face Recognition

This research paper talks about the facial recognition bias which causes the imbalance in the dataset of varied ethnicity [32]. It generates a new dataset from a predefined base dataset using cycle GAN. The dataset generated contains equally distributed four categories of individuals Caucasian, African, Indian, and Asian. The primary objective of this paper is to transform a source image of a particular category into the other three categories by preserving the identity of the individual. In conjunction with the cycle GAN, the images are subjected to three varied loss functions: the Softmax, CosFace, and the Arcface loss as the last layer of the fully connected layer of the neural network.

2.3.4 Automated Skin Tone Extraction for Visagism Applications

This paper states skin tone as a soft biometric component and is generally classified using three skin colors: light, medium, and dark [1]. They have compared the principal component analysis for determining the skin color of a particular region with respect to that of the CNN approach to automatically extract chromatic features from facial images. Upon their evaluation, they have found that the CNN approach obtains an accuracy of 91.29% while the PCA has 86.67%. Since the skin tone is always classified in 3 classes which is not a widely accepted classification scheme my work focuses on classifying it according to Fitzpatrick, which is worldly accepted by various dermatologists across the world.

2.3.5 Fitzpatrick Skin Typing: Applications in Dermatology

Table 2.2: Dermatologist Skin Tone Reading

Fitzpatrick Skin Types	Dermatone Skin Analyzer Reading
Type I	35-50
Type II	50-60
Type III	60-75
Type IV	70-85
Type V	80-100
Type VI	95-127

This paper gives a detailed understanding of the origin of the Fitzpatrick scale and how it has evolved over time [22]. Thomas B. Fitzpatrick developed the Fitzpatrick Scale as a skin classification system for human skin color in 1975. Dermatologists categorizes skin into six Fitzpatrick classes. This classification scheme is used by dermatologists and can be recorded using a device called dermatone skin analyzer [31]. It talks about the effect of sunburn, tanning history, and a genetic disposition with respect to its classes. Table 2.2 gives an idea about how dermatone skin tone readings are labeled under the Fitzpatrick scale and how the scale can help identify six classes of variation with respect to skin color. It also indicates the division of the world population using the six defined classes of skin variations. The Fitzpatrick scale has proven to be effective in diagnosing the patient's level of risk in having a skin disease, sun damage, and skin cancer. Table 2.3 gives the detailed characteristics of Fitzpatrick skin types.

Table 2.3: Fitzpatrick Skin Characteristics for Type I to Type VI

Fitzpatrick Skin Type I	**Fitzpatrick Skin Type II**	**Fitzpatrick Skin Type III**	**Fitzpatrick Skin Type IV**	**Fitzpatrick Skin Type V**	**Fitzpatrick Skin Type VI**
Always burns never tan	Usually burns, minimal tanning	Mild burns at times, uniform tanning	Burns minimally always tans well	Very rarely burns, tans very easily/rapidly	Never tans never burns
The skin color of pale or ivory	Skin color of fair	Skin color of creamy white or fair	Skin color of light brown or olive	Skin color of dark brown to black	Skin color of black
The eye color of blue	Eye color of blue, green, or hazel	Eye color of hazel or light brown	Eye color of brown	Eye color of dark brown to black	Eye color of brownish-black
Hair color of blond or red	Hair color of blonde or red	Hair color of dark blonde to light brown	Hair color of dark brown	Hair color of dark brown to black	Hair color of black
Moderate to severe freckles along the skin	Light to moderate freckles along the skin	Minimal freckling after exposure	Skin doesn't really freckle	Skin doesn't really freckle	Skin doesn't really freckle

Chapter 3

Experiment Design

This chapter covers details about the dataset being used to carry out the experiment design along with the Deep learning neural network architecture which helps in generating the desirable dataset. The results obtained are verified using a widely used open-source facial recognition algorithm “Arcface”.

3.1 Datasets

Data augmentation is defined as a process of adding data to a pre-existing dataset. We have enhanced the Pilot Parliament Benchmark (PPB), IARPA Janus Benchmark–C (IJB-C), and a part of the Morph dataset as the reference point for carrying out the below experiment procedures. PPB dataset [2] gives images of around 1270 individuals with minor variations in the pose. The individuals being public parliamentarians hence justifies the name given. It consists of individuals with both genders from six different countries targeting populations with diversified skin colors. The images in this dataset consist of an average bounding box size of 63 pixels and the IM width and height being 160-590 and 213-886 respectively. The subjects captured in this dataset consists of both African and European countries covering the diversified skin color variations from lighter to dark individuals. Comparing to datasets such as Adience or IJB-A, the PPB dataset gives a uniform distribution of females and males with lighter and darker skin types. 21.3% being darker females, 25% darker males, 23.3% lighter females, and 30.3% lighter males. Subjects in this dataset originate from countries like South-African, Senegal, Rwanda covering darker individuals and lighter from European countries like Sweden, Finland, and Iceland. The metadata which comes along with the dataset has six-points Fitzpatrick classification systems i.e Type I to Type VI as required for the experiment setup thereby giving the ability to pick up an average skin color value for all six-point classes as rated by the dermatologist manually.

Table 3.1: Details about Dataset Being Used

Original Dataset	Total number of Images	Skin labeling
PPB	1270	Available and Dermatologist
IJB-C	31,334	Available and People

The other dataset used is the IJB-C [18] dataset which is the extension of IJB-B with the addition of 1667 new subjects. The total number of subjects included in the dataset is now 3531 with an average of six images per subject a total of 31,334 images out of which 21,294 faces and 10,040 non-faces images. Our enhancement on this dataset is subject to only images and not videos. The images in the dataset consist of diversified populations with full variation in poses. The geographic regions targeted in this dataset include North and South America, Western Europe, South West Africa, East Europe, East Africa, Middle East, Southeast Asia, Indian, China, and East Asia thereby providing images with a vast difference in skin tone color. As the experiment is only focused on the hallucinating skin color of an individual, we only focused on images with skin tone labeled in the metadata. The skin color labeled in the metadata is also subject to the Fitzpatrick classification system which makes it convenient to use. The skin label rating in the metadata is subject to an average rating as rated manually by at least a minimum of nine human raters.

3.2 Beauty GAN: A Generative Adversarial Network

Beauty GAN architecture leverages instance-level facial makeup transfer with deep GAN. It operates on 2 source images: source A and source B. Source A takes the makeup image and source B as the non-make image. The makeup of source A is replicated on the image of source B without changing the facial features. They have tried to achieve the makeup transfer at a domain-level by introducing perpetual loss and cycle consistency loss to maintain the background information. To further extract details at instance-level like extracting color transfer features like eyeliner, lipstick, or foundation they have introduced histogram loss over the particular region of interest. This approach considered the style transfer approach as used by beauty GAN for generating images with 6 different classes of skin tone variation. Here in this experiment the source A images consist of the Fitzpatrick image variation reference templates and source B is the original image whose skin tone variation needs to be achieved. The source A image being the primary factor for analysis, we have considered Figure 3.1 as an input image set.

As stated below in Figure 3.2 the architecture of beauty GAN consists of a generator model that takes Source A Fitzpatrick scale rating template and source B as the input image which has to be transformed. The discriminator accepts the translated image generated by the generator and trains the network with the loss

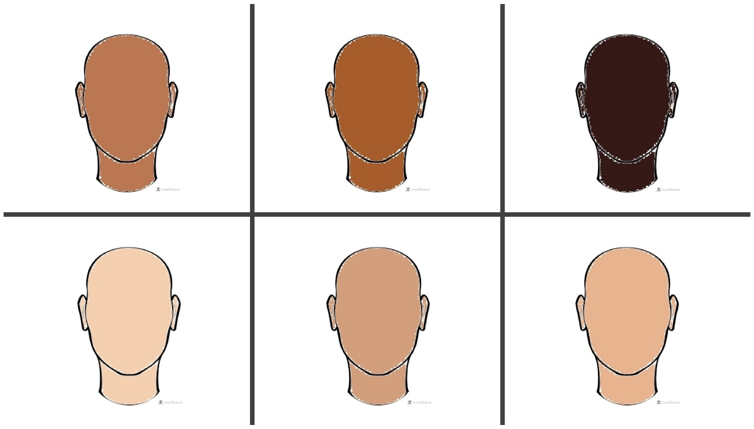

Figure 3.1: Fitzpatrick Skin Images as Source Input

function to distinguish between a real and fake image. The generator G contains 4 types of losses i.e the adversarial loss, cycle consistency loss, skin constrain loss and perceptual loss. Unlike beauty GAN instead of taking makeup attribute as a loss, our project focuses only on the aspect of skin variation of the image thereby considering skin tone loss for training the generator model. The adversarial loss is the summation of the loss of the two discriminators being used to identify the fake and real image differences.

$$L_g = \alpha L_{adv} + \beta L_{cyc} + L_{skin} \tag{3.1}$$

Equation 3.1 refers to the GAN loss equation, where $\mathrm{L_g}$: GAN loss, $\mathrm{L_{adv}}$: adversarial loss which is backpropagated to train the neural network, $\mathrm{L_{cyc}}$: consistency loss, $\mathrm{L_{skin}}$: perpetual loss with respect to skin mask, and α, β represents the weighting factor for each term. The Perpetual loss calculates the high-level feature extracted utilizing the 16-layer VGG network which is pertained on the imagenet dataset. The cyclic consistency loss helps in preserving the image background. The instance-level

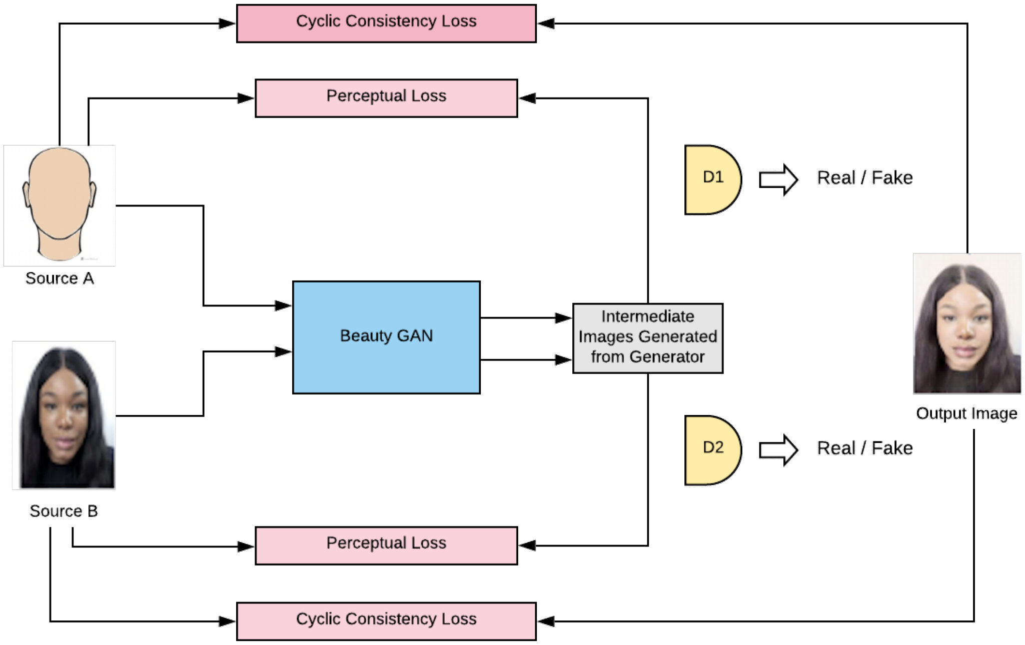

Figure 3.2: Modified Beauty GAN architecture

skin transfer is achieved using histogram loss over the entire image and free parsing is done over the skin region of the entire image.

3.3 Cycle GAN: A Generative Adversarial Network

Cycle GAN as the deep learning neural network is used for designing the experiment plan for generating face images with hallucinating six different variations of skin color starting from light to dark. This architecture addresses the image-to-image translation as it falls into the problem category of computer vision and graphics. Image-to-image transfer approach focuses on the mapping of input image to that of output target image sets. The introduction of cycle consistency loss and back-propagation of these losses to the network architecture drives the performance of cycle GAN architecture to generate more realistic images with respect to two domain classes.

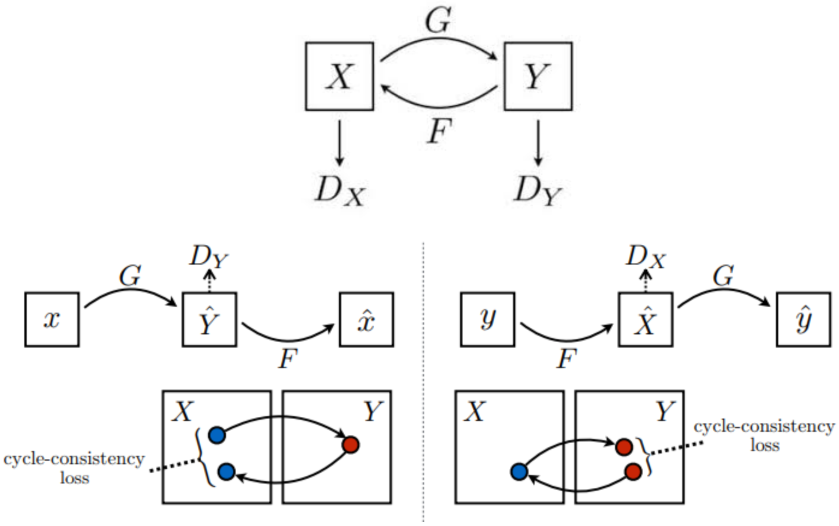

Figure 3.3: Cycle GAN Architecture.
[33]

Figure 3.3 represents the cycle GAN architecture which is used to translate images of one class to another and vice versa [33]. The below mentioned elements provides details about figure implementation of cycle GAN architecture 3.3.

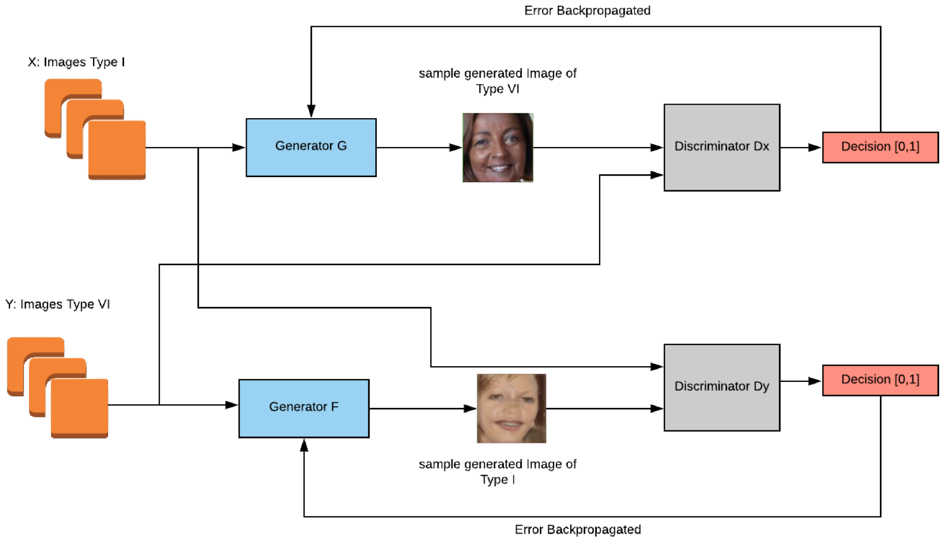

Figure 3.4: Fitzpatrick GAN Architecture for Type I to Type VI.

- G and F indicates the Generator modules.
- D_X and D_Y represents the discriminator modules.
- X and Y are probability distribution of the input domains.
- $\hat{X}$ and $\hat{Y}$ are probability distribution of the generated dataset.
- x and y are single instances from X and Y domain.
- $\hat{x}$ and $\hat{y}$ are single instances of the generated data-sets.

The Generator(G) is used to translate images of Domain X → Y and F from Y → X. Dx and Dy are respective discriminators for class X and Y respectively. We can map this functionality of each generator as G: X → Y and F: Y → X respectively. The output generated by the Generator G i.e G(X) = $\hat{y}$ falls in the same probability distribution as the domain Y and F(Y) = $\hat{x}$ and $\hat{x}$ generated fall into the class X. The

Table 3.2: GAN Training Model Combination

Fitzpatrick class	**Type I**	**Type II**	**Type III**	**Type IV**	**Type V**	**Type VI**
Type I	train(1,1)	train(1,2)	train(1,3)	train(1,4)	train(1,5)	train(1,6)
Type II	train(2,1)	train(2,2)	train(2,3)	train(2,4)	train(2,5)	train(2,6)
Type III	train(3,1)	train(3,2)	train(3,3)	train(3,4)	train(3,5)	train(3,6)
Type IV	train(4,1)	train(4,2)	train(4,3)	train(4,4)	train(4,5)	train(4,6)
Type V	train(5,1)	train(5,2)	train(5,3)	train(5,4)	train(5,5)	train(5,6)
Type VI	train(6,1)	train(6,2)	train(6,3)	train(6,4)	train(6,5)	train(6,6)

discriminator being Dx and Dy encourages the output to fall in the close proximity as that of the probability distribution of the respective domain thereby learning from the fake and real samples error rate produced by the discriminators. This learning of the images is carried out; until the discriminator of the respective class generates an output of 0.5 probability thereby confusing the discriminator between the real and fake samples. In our experiment, the training of the images is done with respect to six classes of skin tone where Type I represents the lightest to Type VI being the darkest skin color. Instead of reconstructing the generated sample, we have focused on using the architecture to only generate face skin tone images of Fitzpatrick skin classes. As the architecture focuses on learning from two classes; the training is thereby performed on the entire combination of all Fitzpatrick classes.

Table 3.2 represents the training model for all the classes starting from Type I to Type VI and the Figure 3.4 represents the architecture used in my experiment to generate images of (Type I, Type VI) training phase. The diagonal training computation as represented in the table 3.2 by names train(1,1), train(2,2), train(3,3), train(4,4), train(5,5) and train(6,6) are invalid as it operates on the same domains. This experiment training only focuses on mutually exclusive training sets. Events like train(1,2) <–> train(2,1) are considered as mutually inclusive and hence are treated as the same training sample. Therefore the training phase is carried out 15 times over all the mutually exclusive combinations of six classes of Fitzpatrick type thereby generating 15 cycle GAN training models to be tested on. To obtain, the skin hallucinated images of the PPB dataset, the testing is carried on each image and the respective skin tone is transferred for the generated model onto the test sets.

3.4 Arc Face: An Open Source Face Matcher

The implementation of biometric systems for security and safety expands the use of FRAs, which are algorithms that extract the facial features of individual captured images and cross-verifies facial features across a predefined template stored in a database. FRAs are predominately used for identification and verification. Arcface [3] which is one of the mostly widely used open-source face matchers has an accuracy of 98%, therefore it was used for analysing the similarity score on the generated images. This helps to understand the impact of bias involved with respect to the skin tone of an individual.

Arcface is a deep convolutional neural network FRA developed in 2018. The primary role of this algorithm is to develop a loss function that extracts discriminative features from images and videos for facial recognition. The proposed approach introduces an additive angular margin penalty to compel intra-class compactness and inter-class discrepancy. Ease of implementation and use, avoidance of complexity for improved performance, and negligible computational complexity are few advantages for choosing Arcface matcher for analyzing the impact of skin tone. The training of this loss function is implemented using various CNN architectures;

our experiment focuses on the pre-trained model of ResNet100 [8]. The training model named MS1M-Arcface alias for ResNet100 is downloaded from the Arcface GitHub [4] repository and is utilized on pre-processed images cropped with a scaling factor of (112 X 112) as per the necessity of this matcher.

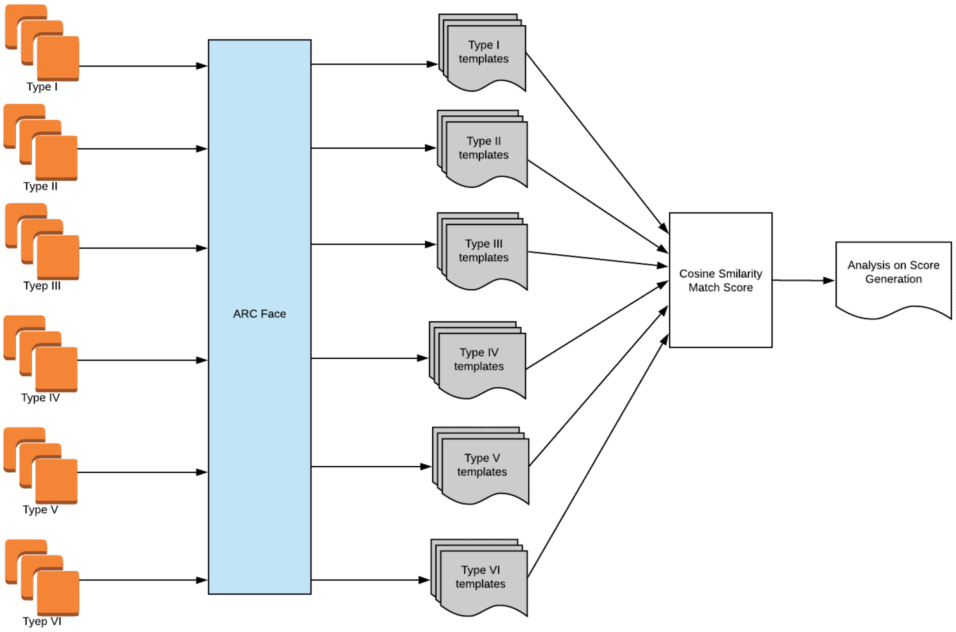

Figure 3.5: Application of Arcface Block Diagram

The accuracy of the ResNet100 architecture has outperformed other CNN architecture used by Arcface matcher. The ResNet module defines the neural network arrangement as a stack which consists of a number of convolution and pooling layers to reduce computational memory usage as well as gaining deep insight about the features in the image samples. The architecture consists of a 100 layer deep arrangement of a pyramidal bottleneck layer of (3 X 3) convolution sandwiched with (1 X 1) convolutions for improved accuracy. The name ResNet refers to the residual units being used and carried over for activation to the next layer of the neural network for detailed feature extraction. The application of ResNet architecture combined with the additive angular loss function of the Arc Face matcher helps in generating templates for each image sample from the dataset. As represented in Figure 3.5 their templates then are used to evaluate the match score of individual identity. If the distance between the match score falls on the higher side of the score ranging from 0-100; it's considered as the same individual. In this experiment, an analysis of the generated match score is then performed to check the involvement of bias with skin tone when the identity of the individual is still being preserved with its facial features.

Chapter 4

Implementation

This chapter covers the necessary experimental procedures, the approach taken and the system requirements utilized to conduct the study.

4.1 Workstation Description

System specifications that drive the experiment requires high computational power due to the use of deep learning neural network architectures. To handle a large amount of image data, we have concurrently utilized multiple resources with Graphics Processing Units (GPU) functionalities. Table 4.1 describes the hardware specifications of these high-end GPUs which are used to train these 15 models as described in Chapter 3. The training is thus performed with the described workstation.

Table 4.1: Workstation Details

Operating System	**Memory**	**Processor**	**Graphics**	**Disk Capacity**
Ubuntu	15.5 GiB	Intel Core i7	GeForce RTX 2060	1.3 TB
Ubuntu	125.6 GiB	Intel Core i7	GeForce RTX 2080	216.5GB

4.2 Software and Libraries

Our experiment setup consists of multiple neural network architectures, one being a GAN for generating skin hallucination images, and other a facial recognition matcher for calculating the authenticity. To access deep learning frameworks for our conducted study, we have used high-end GPU resources for training purpose. Both the architecture uses different configurations for execution and implementation. To manage these cross-platform variations in libraries we have utilized the anaconda cloud virtual environment. Each virtual environment is configured with the below specific requirements.

1. GAN utilizes the below set of libraries and software:
   - python 3.7
   - pytorch 1.3.1
   - cudatoolkit 10.0
   - tourchvision 0.4.2
2. Face Recognition Matcher uses
   - python 3.5.6
   - cudatoolkit 10.2

- mxnet-cu102
- pandas 0.25
- opencv-python 4.2.0

Other generic specifications used for the analysis of results include matplotlib and scipy libraries. The overall end to end coding is developed on a ©PyChram Integrated Development Environment(IDE).

4.3 Experimental Procedure

Changing the skin color of a face image can be performed using various online tools and mobile apps, the manual implementation of this approach to image dataset of more than 1000 images takes an ample amount of time and computational resources. Thereby, automation of this approach by effective utilization of resources available can help us to analyze the impact of skin color variation on the Facial Recognition algorithm. The generated dataset thus created using the automation approach can provide us a platform to mitigate challenges of these open-source algorithms and improve the accuracy, if the images are exposed to the varied controlled environments. These controlled environments can be defined as improper access to light sources; image captured during the night with low resolution etc. An improper capture of the images can result in an increasing number of true negatives thereby denying access to a valid individual. Below are the proposed approaches that we have taken with two different GAN architectures and the modified approach using the cycle GAN architecture, has given us remarkable results for the generated dataset, and has provided key insights when analyzed on the open-source face matcher algorithm.

4.3.1 Proposed Approach

This approach leverages the Beauty GAN architecture for instance-level facial makeup transfer [17] where source A is the make-up image and source B is the non-makeup image on to which the makeup has to be replicated. The idea of this makeup transfer inspired the use of the above architecture on the skin superimposition to the target images. Figure 4.1 is the experimental block diagram designed for this approach.

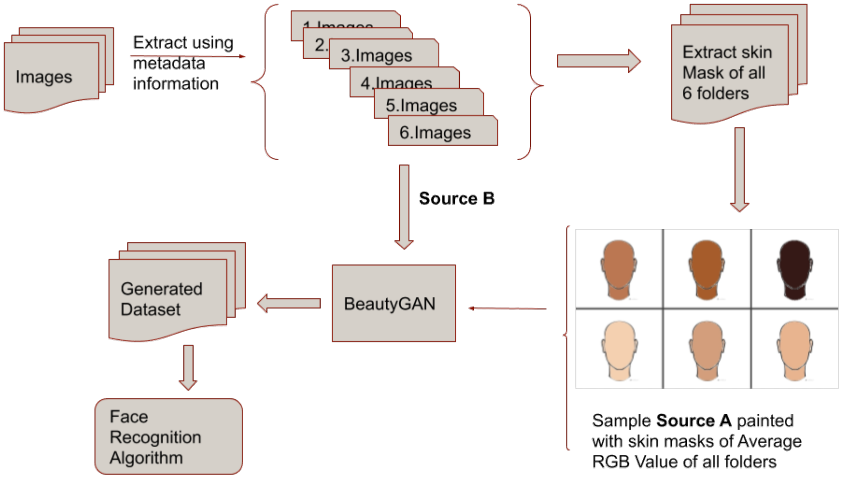
Images
Extract using metadata information
1.Images
2.
3.Images
4.Images
5.Images
6.Images
Extract skin Mask of all 6 folders
Source B
BeautyGAN
Generated Dataset
Face Recognition Algorithm
Sample Source A painted with skin masks of Average RGB Value of all folders

Figure 4.1: Proposed Approach Block Diagram Using Beauty GAN

The beauty GAN architecture for this proposed approach has failed to generate distinguishable skin tone variation images for all six FP classes. Figure 4.2 shows a sample generated image using this approach. By looking at the last image of the generated sample we can conclude that this approach fails to replicate skin color to the target images and thereby showing a change in the background of the image too which was not expected to alter as per the beauty GAN paper.

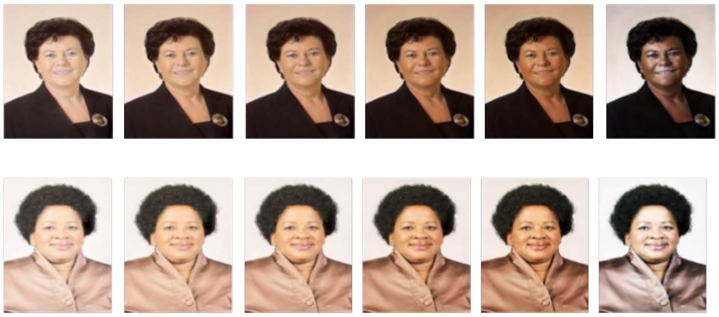

Figure 4.2: Sample Generated Images

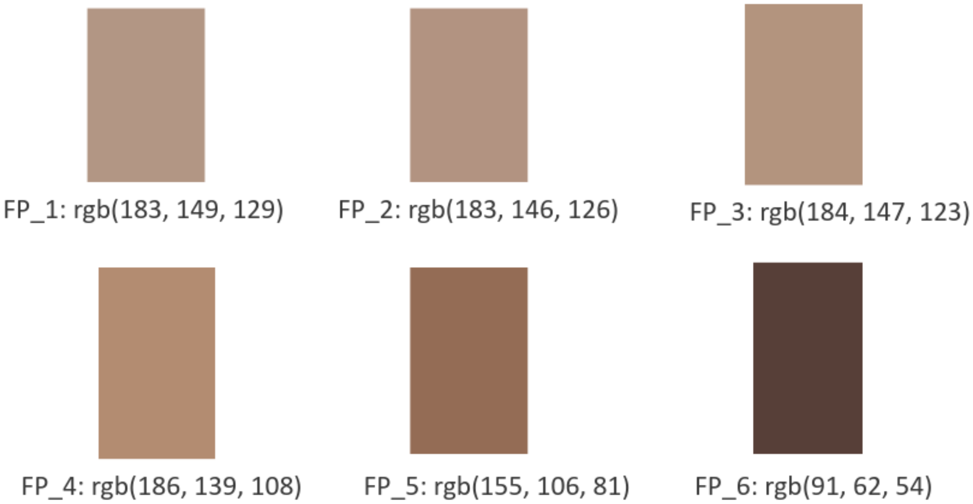

Figure 4.3: Average RGB Value For All Classes of PPB Dataset

As the paper [17] focuses on instant level makeup transfer only i.e. makeup focusing only on lips, eyes, and cheeks; the change of the background didn't carry a proper explanation. The skin masks RGB (red, blue, and green channel) value generated using the average pixel value of face skin images of each separated folders is represented in Figure 4.3. The median of the RGB value with the separated images categorized into six Fitzpatrick classes is illustrated in Figure 4.4. Both the average and median didn't give a clear separation of the first three classes of the Fitzpatrick scale thereby impacting the target generated images.

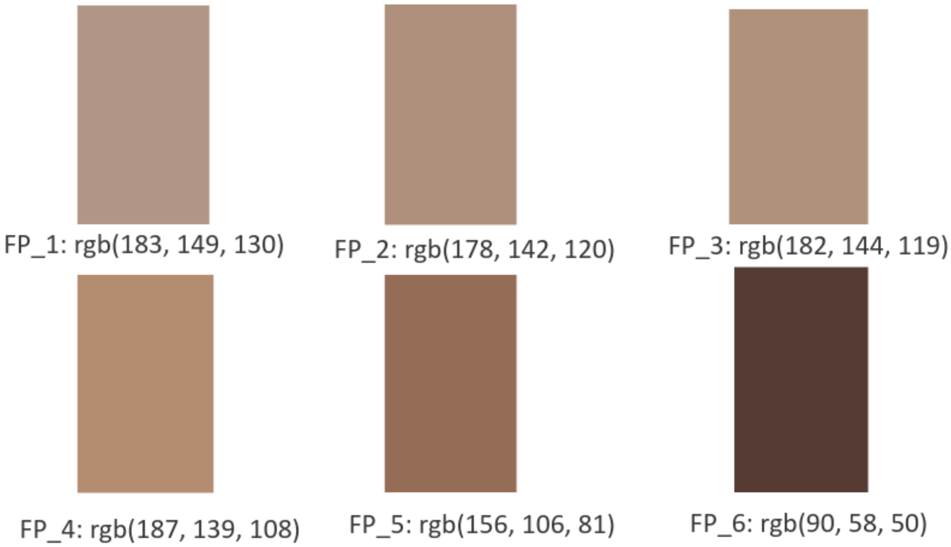

Figure 4.4: Median RGB Value For All Classes of PPB Dataset

4.3.2 Modified Approach

Due to the advancement in deep learning architectures, we have come across various Generative Adversarial Networks. Each advancement to the GANs architecture demonstrated a new way of model generation by changing the basic building block of a GAN architecture. In our modified approach we have considered utilizing the capabilities of cycle GAN architecture, with two generators and two discriminators for transforming images of one class variant into the other [33]. Figure 4.5 represents the process block diagram for the modified approach.

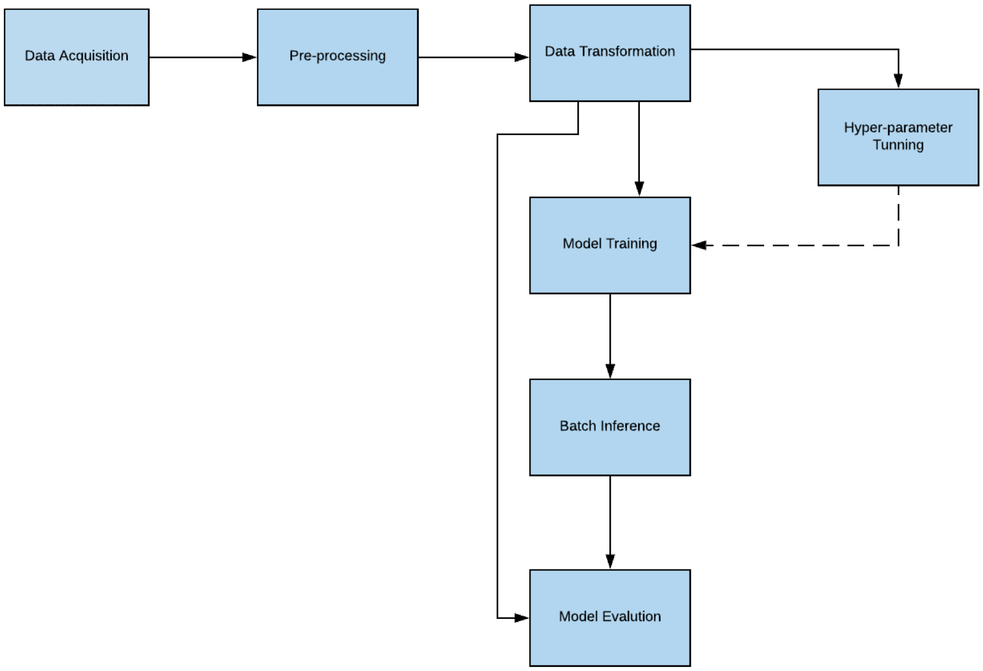

Figure 4.5: Process Block Diagram of Modified Approach

Data acquisition, preprocessing and data transformation can be collectively termed as data-processing. Model training and hyper-parameter decision fall into the category of in-process. Finally, the generated model is tested on a part of the data or an entirely different set of data. In our modified approach, the training and testing are done on different datasets. Evaluation of the generated dataset is done using a Face Recognition Algorithm; the authenticity of the generated images is analyzed by the match scores obtained from the matcher. Each building block as defined by the workflow as in Figure 4.5 carries out a certain specific task as stated below.

- Data Acquisition: A collection of raw data for training and testing
- Pre-processing: Handling the missing data and segregation.

- Data Transformation: Making the raw data training ready i.e. converting it into specific formats as required by the training algorithms.
- Model Training: Training the model with the training dataset
- Hyper-parameter tuning: Find and adjust the training parameters of the model.
- Batch Inference: Testing the trained model with the test dataset.
- Model Evaluation: Analyse model performance by evaluating the images with Face Recognition Algorithm.

Data Pre-processing

Pre-processing of data is referred to as preparing the dataset for training and testing the neural network architectures. These pre-processing steps can be further subcategorized as data acquisition, data handling, and data transformation. Data acquisition refers to the collection of data; this can be achieved by manually downloading images from different internet sources or a predefined set of data that can be downloaded along with the metadata information from a legitimate data repository. Our training and the testing data acquisition is stated below.

- The training data consists of manual downloaded data of almost 336 images each categorized and placed into six Fitzpatrick classes starting from Type I being the lightest to Type VI the darkest skin tone. Each data folder FP class consists of 56 images with one image per subject, randomly picked, and chosen manually by us to fall into the six categories. Few sample images on which the training data is executed along with the folder structure is defined in Figure 4.6.

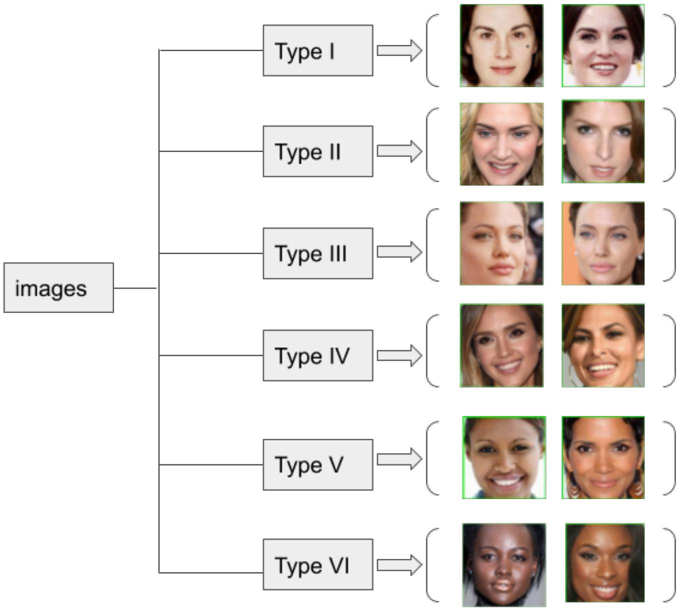

Figure 4.6: Folder Structure Along with Two Sample Images Per Type.

- The test data consists of pre-defined accumulated data as stated in Chapter 3 section 3.1. PPB dataset contains around 1270 images, with a single image per individual. The other dataset used for testing purposes of intra-subject score variation is done on the Morph dataset. This dataset comprises two categories of individuals i.e African Americans with darker skin tone and Caucasians with lighter skin tones. Each subcategory has a combination of males and females subsets. The total number of images in each subset of the Morph group is stated in table 4.2.

Our experiment considers a subset of Morph image manually rated across three human raters. We have considered only the male subset of both groups. As this

Table 4.2: Total Number of Images in Morph Dataset

Group	Number of Images
African American Female (AA$_F$)	5782
African American Male (AA$_M$)	36838
Caucasian Female (C$_F$)	2606
Caucasian Male (C$_M$)	8005

dataset doesn't have metadata information with skin color rating, we have taken a subset of individuals in both the groups which were manually labeled as category 1 and category 6 across 3 human raters. With this data approach, we have selected 417 unique subjects from the AA_M group and 944 subjects from C_M. Each group has a total number of 2435 and 4398 images. Hence, giving rise to more than one image per subject for intra-subject score analysis. Figure 4.7 are few image sample of the PPB datasets on which data augmentation is performed using our modified approach and figure 4.8 represents the images for intrasubject score variations analysis from the Morph dataset.

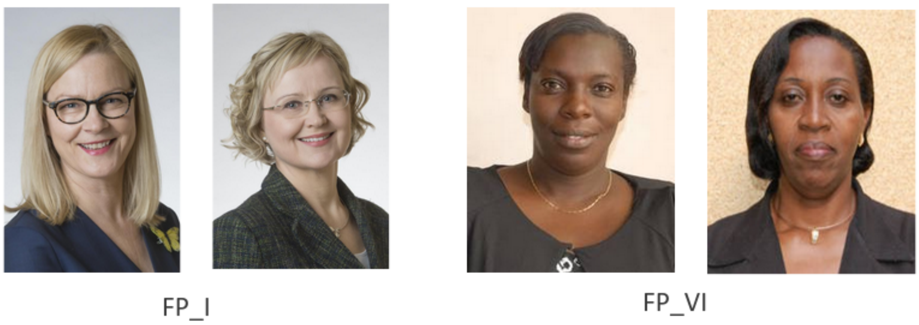

Figure 4.7: PPB Dataset Sample Images

Before the execution of the training phase using deep learning architecture, the training and the testing data are pre-processed with face image being loosely cropped. Other pre-processing steps include image resizing to a uniform variant

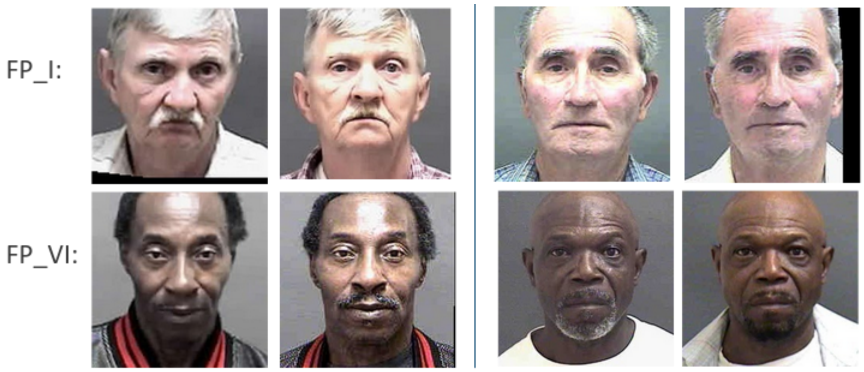

Figure 4.8: Morph Dataset Sample Images

of (112 X 112) dimension as accepted by both neural networks as well as the face matcher algorithm. The entire image cannot be subjected to training purposes as the neural network would learn details about the background of the image which is not relevant for our study. Segregation of images into six Fitzpatrick categories, neglecting downloaded images that fail to detect a face, and handling other outliers are a part of data handling and transformations.

In-processing

In-process is referred to as the training phase of a deep learning neural network architecture. This phase is usually computationally expensive as it utilizes the software and hardware capabilities of the system to learn details about images. Image processing and feature extraction are carried out on all the pre-processed images using the deep adversarial architecture. In the presented experimental setup, we focused on training the neural network with 15 combinations as stated in Chapter 3 section 3.2. Figure 4.9 represents the in-process block diagram of the cycle GAN architecture. The left side of the figure 4.9 describes the training phase, where the cycle GAN takes two class inputs and generates checkpoints for each combination.

After running the experiment with different epochs ranging from 100 to 600, we have finalized the below hyper-parameters configuration. Table 4.3 gives a key insight into the tuning details.

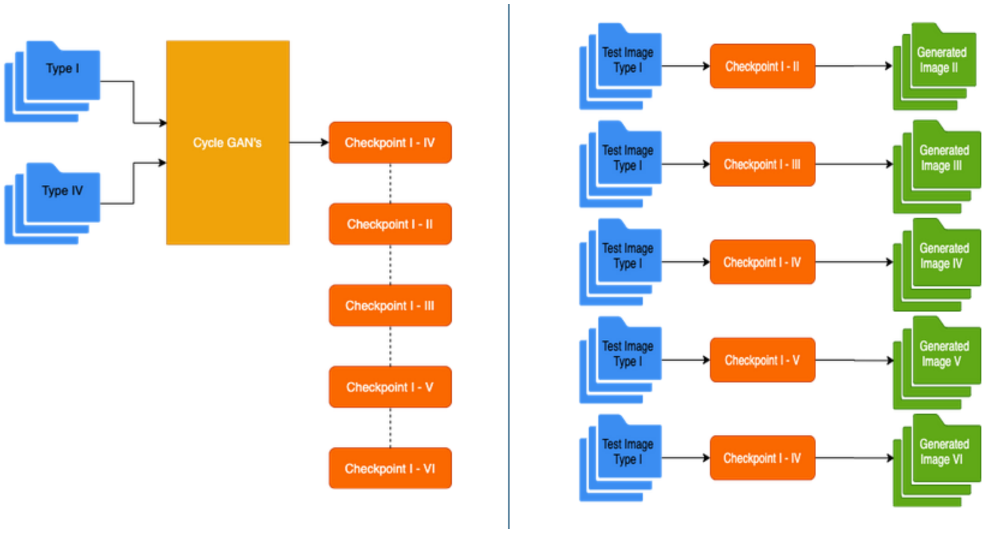

Figure 4.9: Modified Approach Testing and Training Phase Block Diagram

The 15 checkpoints thus generated after training cycle GAN model are located in the folder structure as represented below. Each file named "latest.ckpt" as stated in Figure 4.10 defines the weights and biases learned by training on the six dataset folders of different skin shades. These generated checkpoints are used to transform images on the test datasets. On the right of figure 4.9, describes the testing phase of the generation process where a checkpoint is used to transform skin tone belonging to two different classes. Our approach focuses on only FP-1 and FP-6 combinations thereby generating a total of 9 checkpoints on which transformation is carried out.

Table 4.3: Hyper-Parameter Details for Training Model

Hyper-parameters Name	**Detail**
Epochs	600
Decay Epoch	100
Batch Size	1
Learning Rate	0.002
Load Height	286
Load Width	286
Crop Height	256
Crop Width	256
Load Height	286
lambda	10
IDT co-efficient	0.5
Load Width	286
Normalization	Batch
Drop Out	No drop out for Generator
Number of Generator filter in 1st Convolution	64
Number of Discriminator filter in 1st Convolution	64

Post-processing

Post-processing of data in machine learning algorithms refers to cleaning and removing noisy data from the generated dataset. This step is usually carried out after the training phase of the model generation. In our experiment post-processing focuses on applying the generated GANs model on the dataset like PPB dataset with 1270 images and Morph subcategories of AA_M and C_M of 417 and 944 unique subjects. A test script to run on the entire folders of the test data is executed and the respective skin variation images of each individual are placed in the folder categorized as [1, 2, 3, 4, 5, 6]. If the original image is marked as class 1 image, then the respective 2, 3, 4, 5 and 6 Fitzpatrick skin color image is obtained by

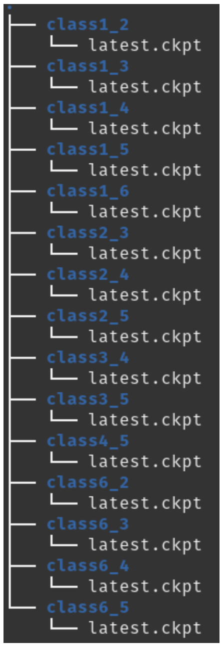

```
.
├── class1_2
│   └── latest.ckpt
├── class1_3
│   └── latest.ckpt
├── class1_4
│   └── latest.ckpt
├── class1_5
│   └── latest.ckpt
├── class1_6
│   └── latest.ckpt
├── class2_3
│   └── latest.ckpt
├── class2_4
│   └── latest.ckpt
├── class2_5
│   └── latest.ckpt
├── class3_4
│   └── latest.ckpt
├── class3_5
│   └── latest.ckpt
├── class4_5
│   └── latest.ckpt
├── class6_2
│   └── latest.ckpt
├── class6_3
│   └── latest.ckpt
├── class6_4
│   └── latest.ckpt
└── class6_5
    └── latest.ckpt
```

Figure 4.10: Checkpoint Directory Structure

utilizing the class1_2, class1_3, class1_4, class1_5, and class1_6 checkpoints respectively. This entire set of execution is performed on all the images, categorized into different Fitzpatrick types.

After the generation of the two new datasets, cleansing of noisy data before performing a facial recognition analysis is carried out. This cleansing includes removing images from all the datasets which are a failure to detect cases with the Arcface matcher. Hence, giving us a refined dataset for evaluation and analysis. As stated in chapter 3 section 3.3 the generated dataset is then compared with the original dataset using the Arcface matcher to check if the skin color plays a significant role to increase the true negatives in Facial Recognition Algorithms. Since the PPB dataset only comprises one image per subject, an intra-subject score analysis can't be performed on this particular dataset. Morph dataset thus plays a significant role in giving us the necessary takeaway with intrasubject score analysis. The implementation procedure thus gives us a clear idea of the benefit of GAN architecture, thereby giving us the flexibility to augment data to a pre existing dataset and draw analysis on the impact of the skin tone affecting facial recognition algorithms.

4.4 Significance of Box Plots

The box plot provides a means of representing the distribution of data across a common axis. This can be summarized using 5 points: minimum, maximum, first quartile (Q1), third quartile (Q3), and median [5]. Figure 4.11 shows the different parts of a box plot.

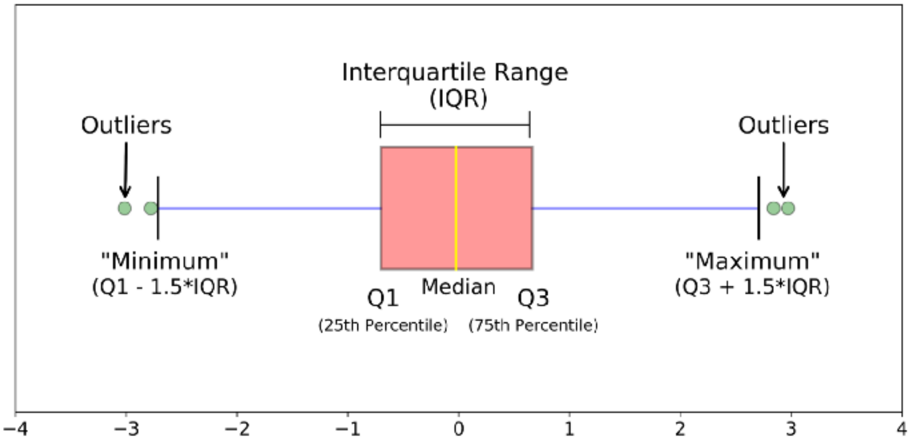

Figure 4.11: Different Parts of a Box Plot

- First Quartile/Q1: Represents the numbers between the smallest number and the median value or in other words the 25th percentile.
- Median/Q2: Represents the middle value of the dataset or in other words the 50th percentile.

- Third Quartile/Q3: Represents the numbers between the largest number and the median value or in other words the 75th percentile.
- Interquartile Range(IQR): Highlights the maximum distribution of points in the dataset which is from 25th to 75th percentile.
- Maximum and Minimum: Represent the outlier of the entire distribution and is calculated with the formula as shown in figure 4.11.

This plot has been a boon to analyze the score distribution generated by the comparison of two images, the original when being compared with the other five generated Fitzpatrick class images. Plotting probability distribution plots for all classes would be of more beneficial to visualize the impact of skin tone when changed from light to dark. This plot gives us the flexibility to plot all the class variation in a single locality. Matplotlib python is used to generate the plots.

4.5 Significance of Cosine Similarity

Images are represented in three-dimensional vectors. FRAs use the vectors to generate a template for each image with facial features. Cosine similarity is generally used to measure the correlation between templates generated using CNNs. A match score, computed after the template comparison, is the euclidean distance for checking authenticity. Image-to-image comparison requires cosine similarity in order to find the smallest angular difference between two image templates. The higher the score generated using this comparison technique, the more similar are the two feature vectors of the images. Python libraries like scipy are used to compute the cosine similarity scores of two feature vectors.

Chapter 5

Results

This chapter gives a detailed analysis of the key points of the conducted study. The training set for the FRAs typically contains images of mostly Caucasians. This bias results in higher false match rates with respect to darker skin tones. To eradicate the impact of skin color bias, our experiment focused on generating datasets with diversified skin tones. The evaluation of the generated dataset includes analyzing the impact of skin colors on the open-source matcher algorithm. An explanation of the important box plots is generated to evaluate the results.

5.1 Analysis on PPB Dataset

Figure 5.1 represents the cosine similarity match scores generated in text files using the Arcface matcher. Column 1 represents the ID of the image template. Column 2 indicates the match score of the probe, which is the original image, with itself, resulting in a similarity score of 100.0. Columns 3 to 7, named "gen_2," "gen_3," "gen_4," "gen_5," and "gen_6," show the probe comparison scores of the generated cycle GAN skin hallucinated images. From the metadata, the probe is rated as FP-1. Sample images as in figure 5.2 are generated using our modified approach.

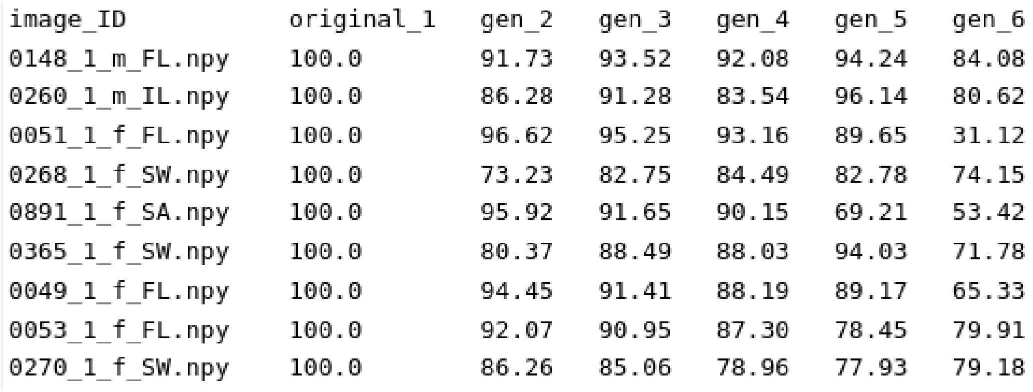

```
image_ID          original_1    gen_2    gen_3    gen_4    gen_5    gen_6
0148_1_m_FL.npy   100.0         91.73    93.52    92.08    94.24    84.08
0260_1_m_IL.npy   100.0         86.28    91.28    83.54    96.14    80.62
0051_1_f_FL.npy   100.0         96.62    95.25    93.16    89.65    31.12
0268_1_f_SW.npy   100.0         73.23    82.75    84.49    82.78    74.15
0891_1_f_SA.npy   100.0         95.92    91.65    90.15    69.21    53.42
0365_1_f_SW.npy   100.0         80.37    88.49    88.03    94.03    71.78
0049_1_f_FL.npy   100.0         94.45    91.41    88.19    89.17    65.33
0053_1_f_FL.npy   100.0         92.07    90.95    87.30    78.45    79.91
0270_1_f_SW.npy   100.0         86.26    85.06    78.96    77.93    79.18
```

Figure 5.1: First 10 Subject Scores from PPB Dataset categorized as Type I

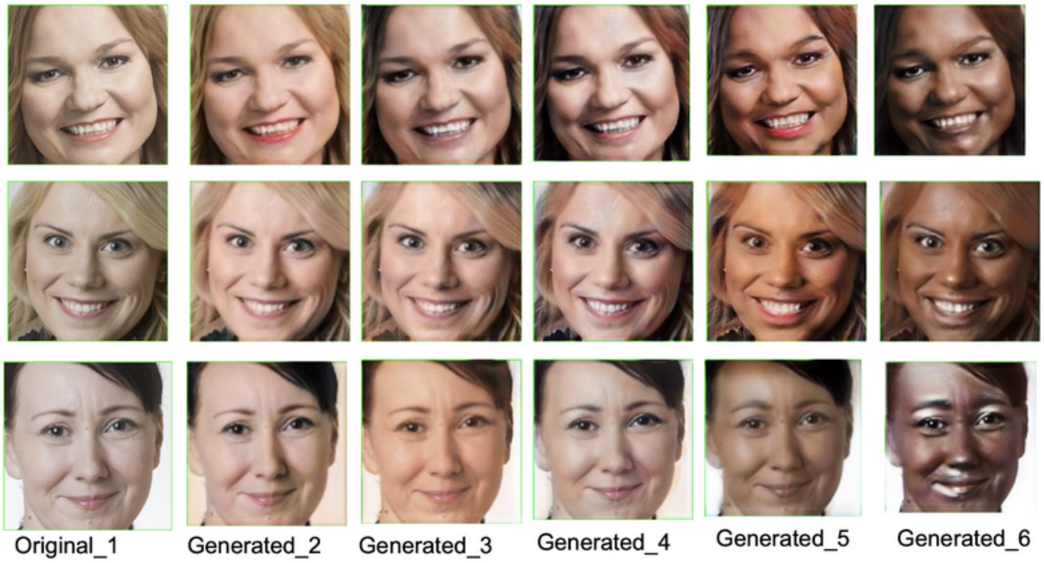

Figure 5.2: Sample Generated Images Categories as FP-1

The generated text file represented in figure 5.1 is plotted in figure 5.3, which summarizes the scores in a single locality. A huge drop in score distribution occurs when an original image is compared with the darkest skin color of the same image even after preserving facial features across the skin hallucinated images. The plot in figure 5.3 has some outliers (indicated with circles), "gen_2," "gen_4," and "gen_5" with scores below the usual distribution. A sample of the low-scoring images is represented in figure 5.4 along with the scores. The few low-scoring images are failed cases that indicate the induced factors from the training datasets. Unwanted effects can be improved with proper uniform distribution of the images in the training phase.

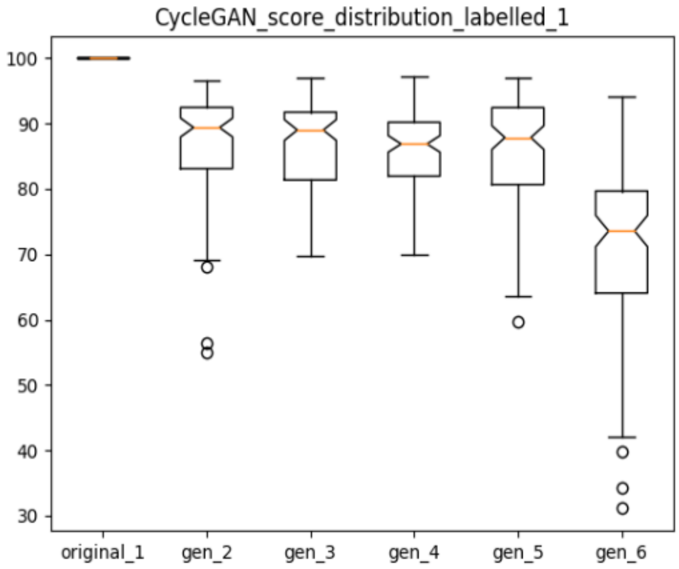

Figure 5.3: Box Plot for PPB Dataset Categorized as Type I

Figure 5.5 represents the mean and standard deviation of the original and generated images. The first row is preserved in the table to give a detailed comparison.

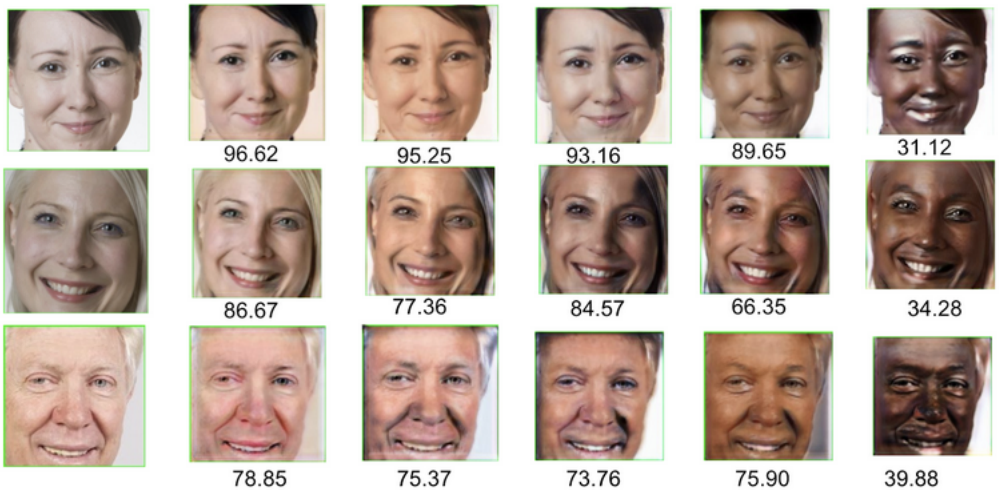

Figure 5.4: Low Score Outlier Samples from PPB FP-1

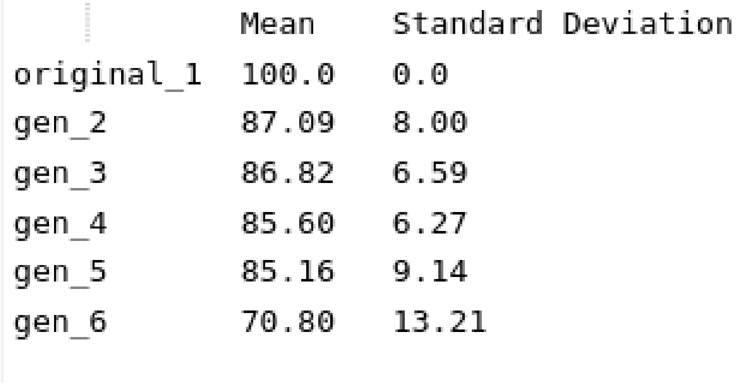

```
             Mean    Standard Deviation
original_1   100.0   0.0
gen_2        87.09   8.00
gen_3        86.82   6.59
gen_4        85.60   6.27
gen_5        85.16   9.14
gen_6        70.80   13.21
```

Figure 5.5: Mean and Standard Deviation Distribution for PPB Type I

Images rated FP-6 as per PPB metadata, which are the probes with image IDs listed in column 1 of the figure 5.6, are plotted against the match scores when compared to the generated images that fall in category 1 to 5. Figure 5.7 shows a few image samples on which the comparison is performed. Original_6 of figure 5.7 represents the probe comparison to itself and column 2 to 1 represents the score for generated images.

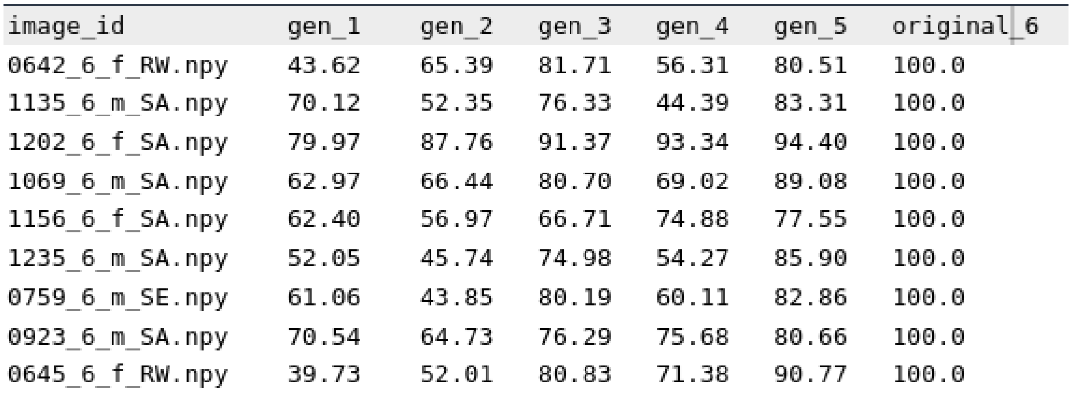

image_id	gen_1	gen_2	gen_3	gen_4	gen_5	original_6
0642_6_f_RW.npy	43.62	65.39	81.71	56.31	80.51	100.0
1135_6_m_SA.npy	70.12	52.35	76.33	44.39	83.31	100.0
1202_6_f_SA.npy	79.97	87.76	91.37	93.34	94.40	100.0
1069_6_m_SA.npy	62.97	66.44	80.70	69.02	89.08	100.0
1156_6_f_SA.npy	62.40	56.97	66.71	74.88	77.55	100.0
1235_6_m_SA.npy	52.05	45.74	74.98	54.27	85.90	100.0
0759_6_m_SE.npy	61.06	43.85	80.19	60.11	82.86	100.0
0923_6_m_SA.npy	70.54	64.73	76.29	75.68	80.66	100.0
0645_6_f_RW.npy	39.73	52.01	80.83	71.38	90.77	100.0

Figure 5.6: First 10 Subject Scores from PPB Dataset Categorized as Type VI

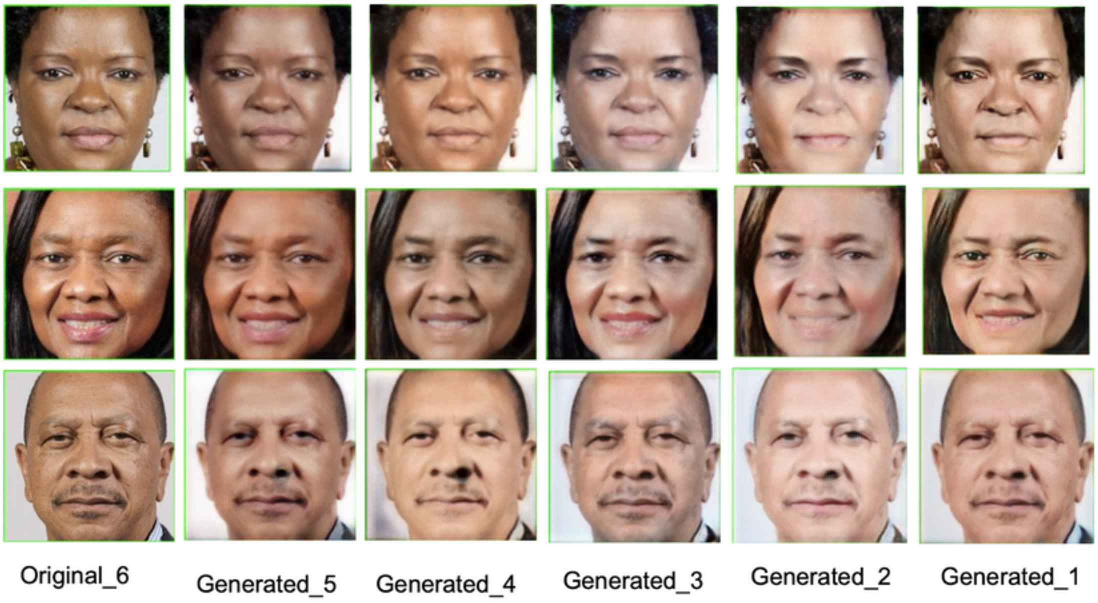

Figure 5.7: Sample Generated Images Categories as FP-6

The box plot for Type VI PPB data distribution is shown in figure 5.8. A drop in the scores of the testing samples is noted when images with darker skin are converted to ones with lighter, but the drop may not be consistent due to the impact of the training models.

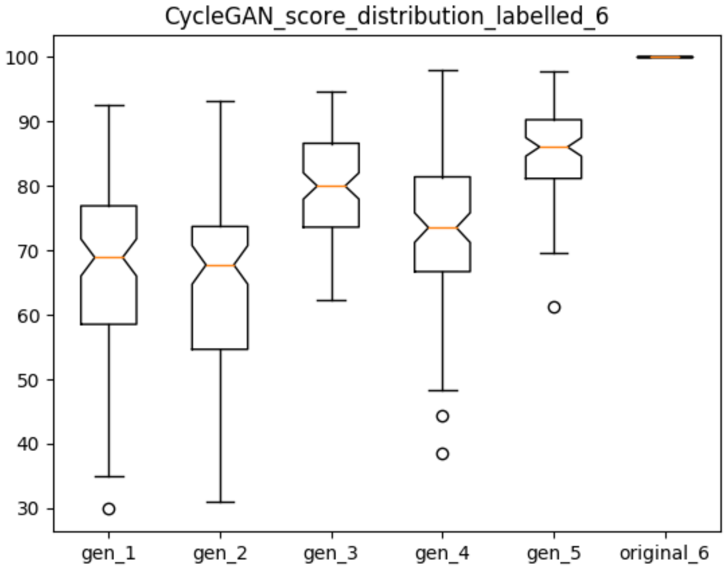

Figure 5.8: Box Plot for PPB Datasets Categorized as Type VI

Low scoring outliers of the testing samples, which indicate a drop in scores, are marked in red as shown in figure 5.9.

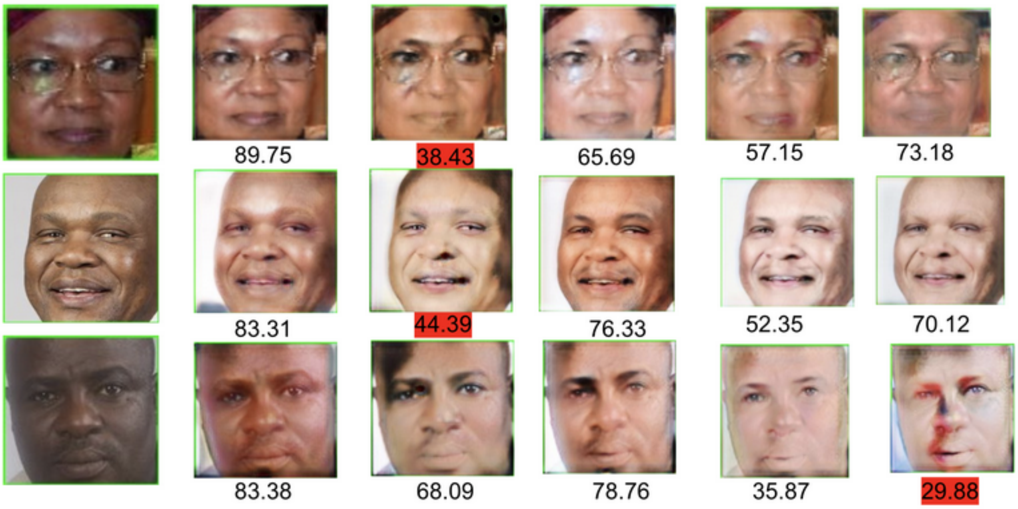

Figure 5.9: Low Score Outlier Samples from PPB FP-6

The mean and standard deviation of PPB Type VI score distribution is displayed in figure 5.10.

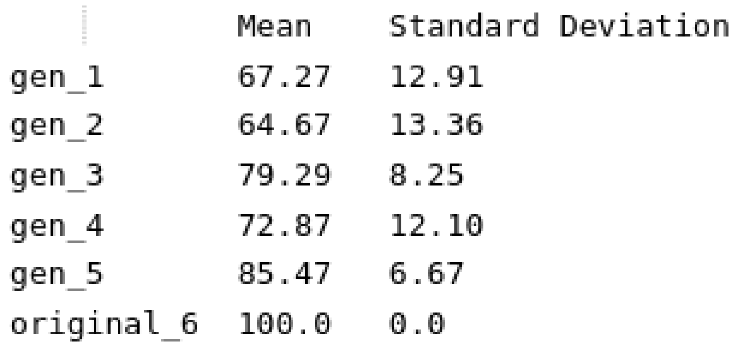

```
            Mean    Standard Deviation
gen_1       67.27   12.91
gen_2       64.67   13.36
gen_3       79.29   8.25
gen_4       72.87   12.10
gen_5       85.47   6.67
original_6  100.0   0.0
```

Figure 5.10: Mean and Standard Deviation Distribution for PPB Type VI

5.2 Analysis of Morph Caucasian

The morph Caucasian dataset consists of at least two images per subject, allowing the flexibility to analyze the impact of skin color when modified across all the images of the same subject.

Figure 5.11 displays the scores generated in a comparison of the probe with each generated image in the morph dataset. “subject1image1” from the original set is compared with “subject1image1” of the generated classes 2, 3, 4, 5, and 6. The “original_1” column reveals the probe comparisons with themselves that produce a similarity score of 100.0.

The mean and standard deviations are shown in figure 5.12. The standard deviations indicate a consistent increase in score distribution across class Types IV, V, and VI whereas Types I, II, and III have less variation.

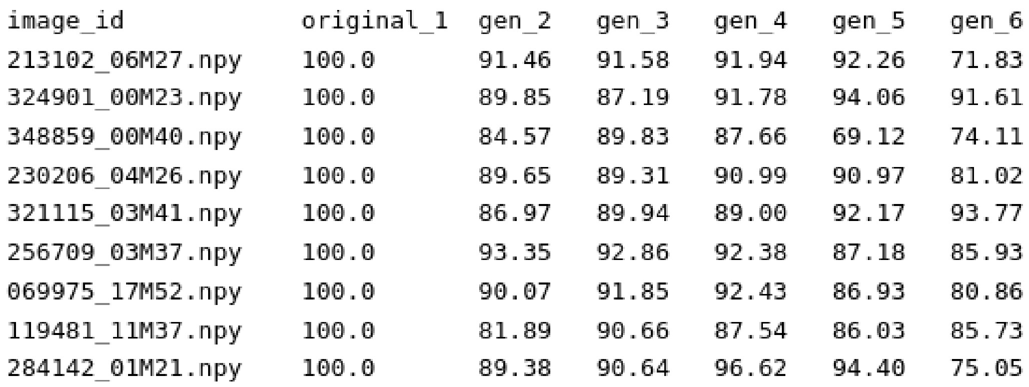

```
image_id            original_1  gen_2   gen_3   gen_4   gen_5   gen_6
213102_06M27.npy    100.0       91.46   91.58   91.94   92.26   71.83
324901_00M23.npy    100.0       89.85   87.19   91.78   94.06   91.61
348859_00M40.npy    100.0       84.57   89.83   87.66   69.12   74.11
230206_04M26.npy    100.0       89.65   89.31   90.99   90.97   81.02
321115_03M41.npy    100.0       86.97   89.94   89.00   92.17   93.77
256709_03M37.npy    100.0       93.35   92.86   92.38   87.18   85.93
069975_17M52.npy    100.0       90.07   91.85   92.43   86.93   80.86
119481_11M37.npy    100.0       81.89   90.66   87.54   86.03   85.73
284142_01M21.npy    100.0       89.38   90.64   96.62   94.40   75.05
```

Figure 5.11: First 10 Subject Scores from Morph C_M Categorized as Type I

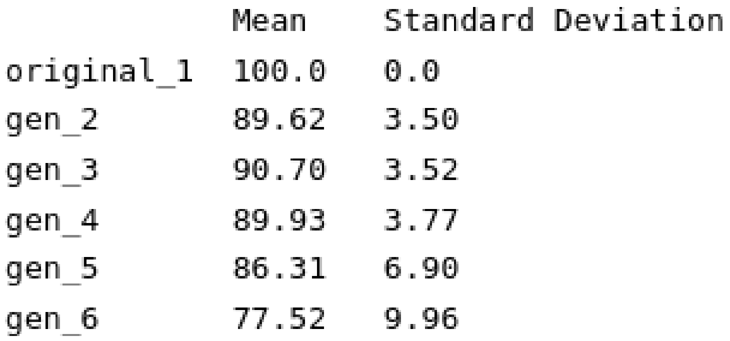

```
             Mean    Standard Deviation
original_1   100.0   0.0
gen_2        89.62   3.50
gen_3        90.70   3.52
gen_4        89.93   3.77
gen_5        86.31   6.90
gen_6        77.52   9.96
```

Figure 5.12: Mean and Standard Deviation Distribution for C_M Type I

A few sample images generated from the morph Caucasians are represented in figure 5.13. The images to the extreme left is a combined rating of three human raters as FP-1. The other columns are the generated images using our modified approach with the same training set. Due to less number of training image samples and variation in the type of images, the GAN failed to generate better sample when tested on Morph subjects.

The box plot presented in Figure 5.14 is an intra-subject score analysis for each for Caucasian male labeled as Type I. “gen_2,” “gen_3”, “gen_4”, “gen_5,”, and “gen_6” are the generated images for the “original_1” probe. The score plotted is

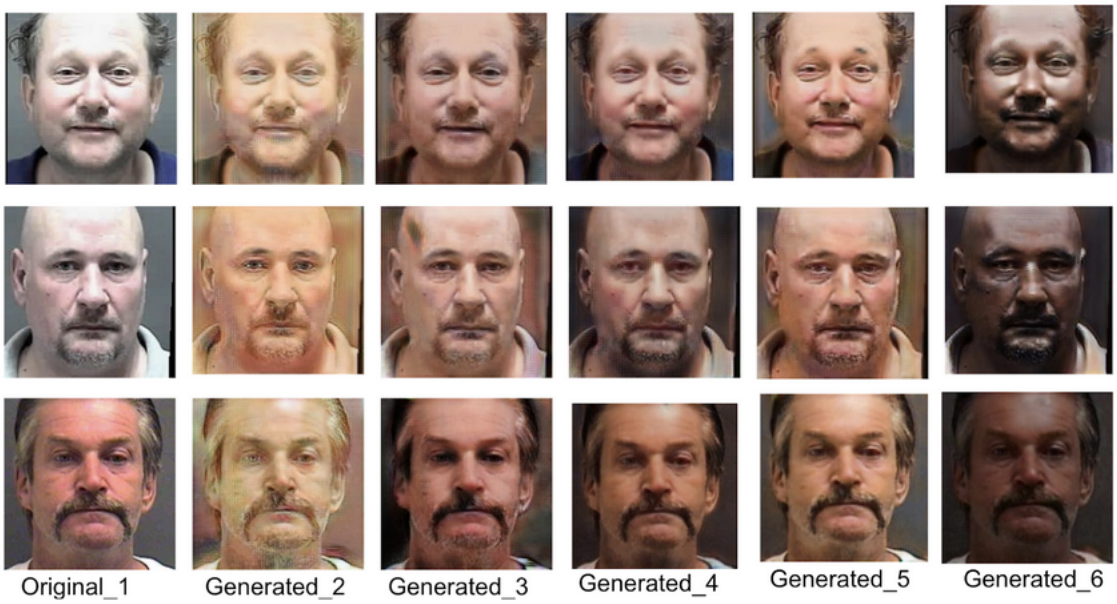

Figure 5.13: Sample Generated Images Categories as FP-1

a comparison between multiple samples of the same subjects. Assuming subject1 has three images taken with different intervals of controller environment at different time intervals. Match score is generated with a different sample of the same subject within each generated category of classes 2, 3, 4, 5, and 6. An example comparison is stated as (subject1Image1, subject1Image2), (subject1Image1, subject1Image3) and (subject1Image2, subject1Image3) of the same type class. The original_1 box plot sample represents the intra-subject score comparison of each subject. Analyzing the box plot for morph Caucasian we see a uniform distribution drop in scores for every class which signifies that the generated images are less affected by the GAN architecture. On the other hand, the drop in score in the “gen_6” might signify the effect of skin tone as a crucial factor for non-uniformity. But any conclusive statement would need further investigation with improved dataset.

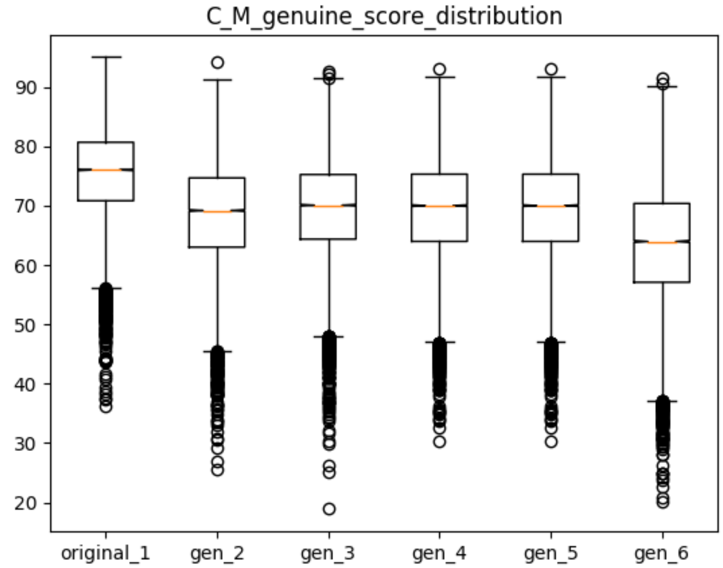

Figure 5.14: Box Plot for C_M Genuine Intra Subject

Figure 5.15 plots a cross intra-subject analysis. Assuming subject1 with three images per subject at different intervals of time and environment; the match scores are generated with a cross image comparison of original intra subjects with that of the generated ones. The sample comparisons of subject 1 with three images are:

- (subject1Image1_original1, subject1Image2_gen2)
- (subject1Image1_original1, subject1Image3_gen2)
- (subject1Image2_original1, subject1Image1_gen2)
- (subject1Image2_original1, subject1Image3_gen2)
- (subject1Image3_original1, subject1Image1_gen2),
- (subject1Image3_original1, subject1Image2_gen2)

The “original_1” plot represents same probe with different images.

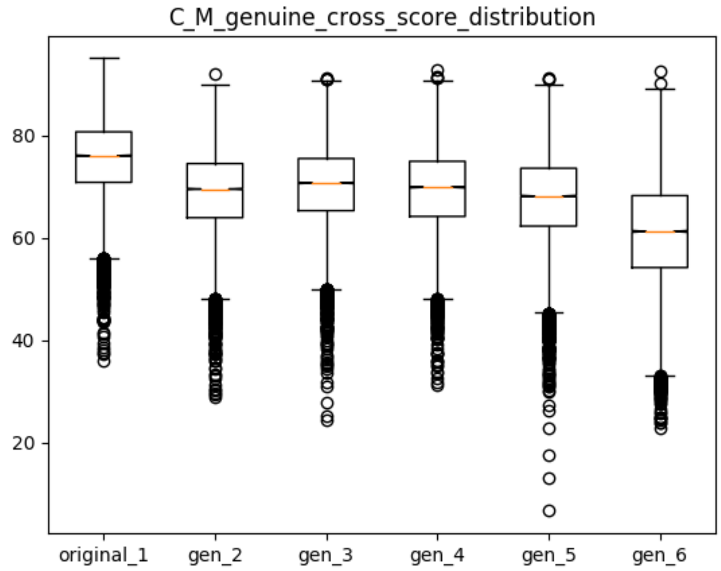

Figure 5.15: Box Plot for C_M Genuine Cross Intra Subject

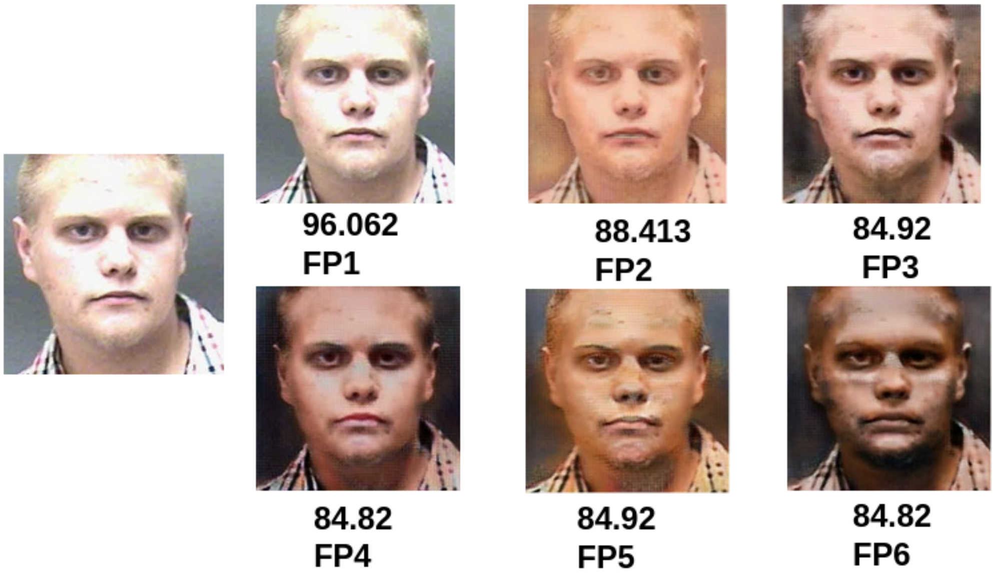

Figure 5.16: High scoring sample

Figure 5.16 is an image from the morph Caucasian dataset which scores high with the intrasubject analysis. The scores observed are consistently high.A low scoring subject is shown figure 5.17 . Scores are uniformly under the threshold with an original and generated comparison. Factors like other facial features which include the length of beard, no mustache affect the similarity score and eliminates the idea of GAN causing the drop in score.

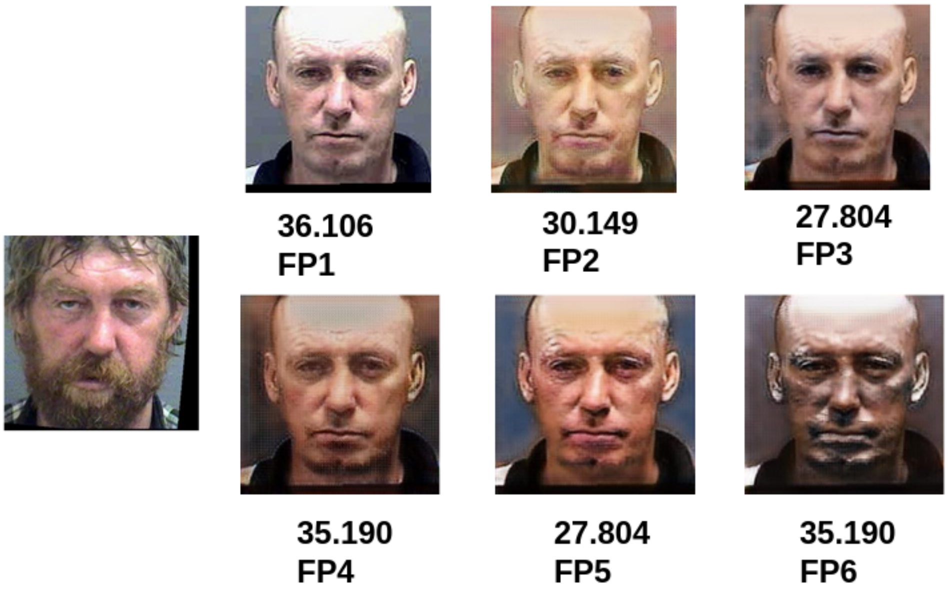

Figure 5.17: Low scoring sample

5.3 Analysis for Morph African American

Subjects chosen for the plot are African American subset from morph dataset, categorized as skin tone Type VI when rated with 3 human raters. The original_6 probe are matched against generated 1, 2, 3, 4, and 5 as shown in figure 5.18. Sample images for this generated dataset can be seen in figure 5.19. The impact of lip color on certain images indicates the increased number of female subjects in the training set.

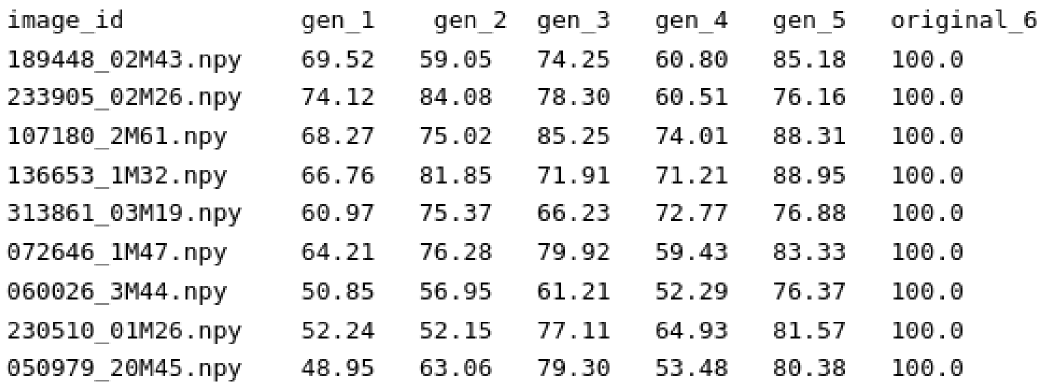

```
image_id            gen_1    gen_2  gen_3   gen_4   gen_5   original_6
189448_02M43.npy    69.52   59.05   74.25   60.80   85.18   100.0
233905_02M26.npy    74.12   84.08   78.30   60.51   76.16   100.0
107180_2M61.npy     68.27   75.02   85.25   74.01   88.31   100.0
136653_1M32.npy     66.76   81.85   71.91   71.21   88.95   100.0
313861_03M19.npy    60.97   75.37   66.23   72.77   76.88   100.0
072646_1M47.npy     64.21   76.28   79.92   59.43   83.33   100.0
060026_3M44.npy     50.85   56.95   61.21   52.29   76.37   100.0
230510_01M26.npy    52.24   52.15   77.11   64.93   81.57   100.0
050979_20M45.npy    48.95   63.06   79.30   53.48   80.38   100.0
```

Figure 5.18: First 10 Subject Scores from Morph AA_M Categorized as Type VI

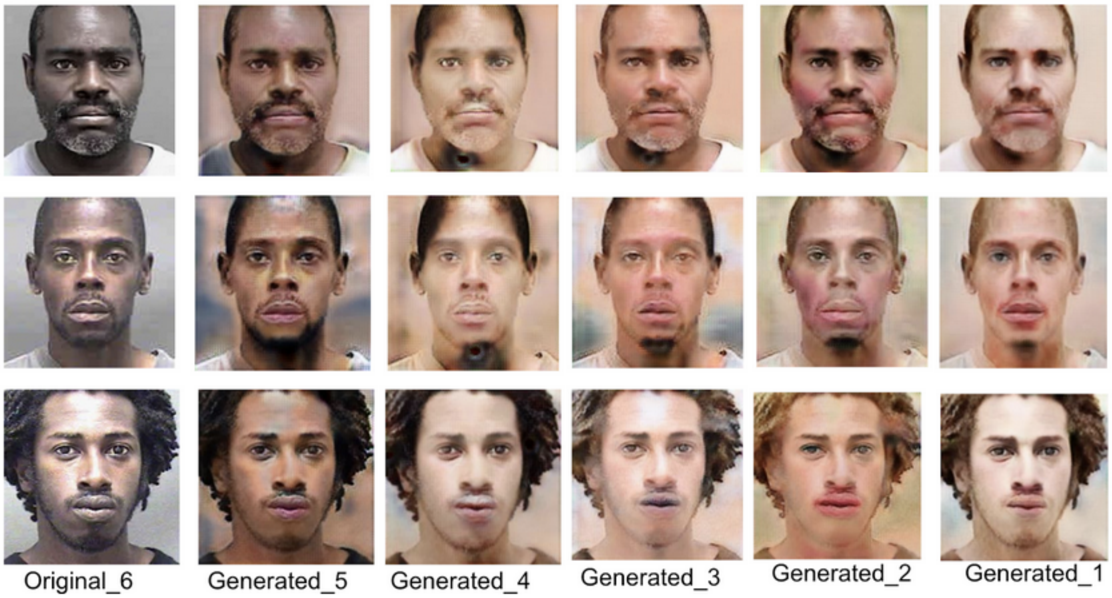

Figure 5.19: Sample Generated Images Categories as FP-6

The mean and standard deviations for original and generated images are illustrated in figure 5.20.

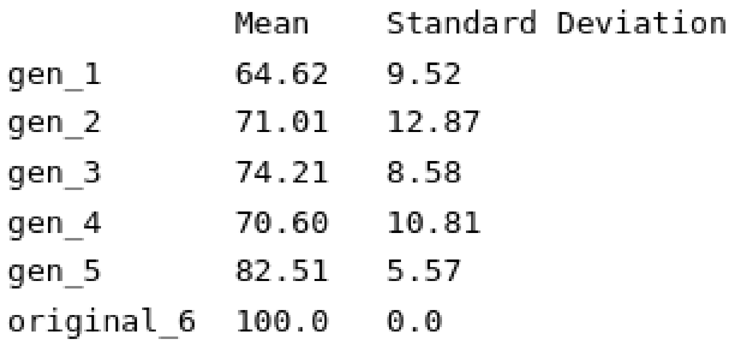

```
             Mean    Standard Deviation
gen_1        64.62   9.52
gen_2        71.01   12.87
gen_3        74.21   8.58
gen_4        70.60   10.81
gen_5        82.51   5.57
original_6   100.0   0.0
```

Figure 5.20: Mean and Standard Deviation Distribution for AA_M Type VI

The genuine intra-subject score analysis for morph African American group is shown in figure 5.21. The images categorized as Type VI is compared with the generated images of types I to V. Considering the three images of subject 1, the comparison is as follows.

- (subject1Image1, subject1Image2)
- (subject1Image1, subject1Image3)
- (subject1Image2, subject1Image3)

"original_6" in X-axis of the box plot in figure 5.22 gives the idea of match score distribution for probe intra-subject feature matching. "gen_1," "gen_2," "gen_3," "gen_4," and "gen_5" are intra-subject scores of each categories respectively.

The box plot shown in figure 5.22 is the intra-subject genuine comparison between original and the generated type classes. The combinations of two types of classes, with same subject different images, are as follows:

- (subject1Image1_original6, subject1Image2_gen2)

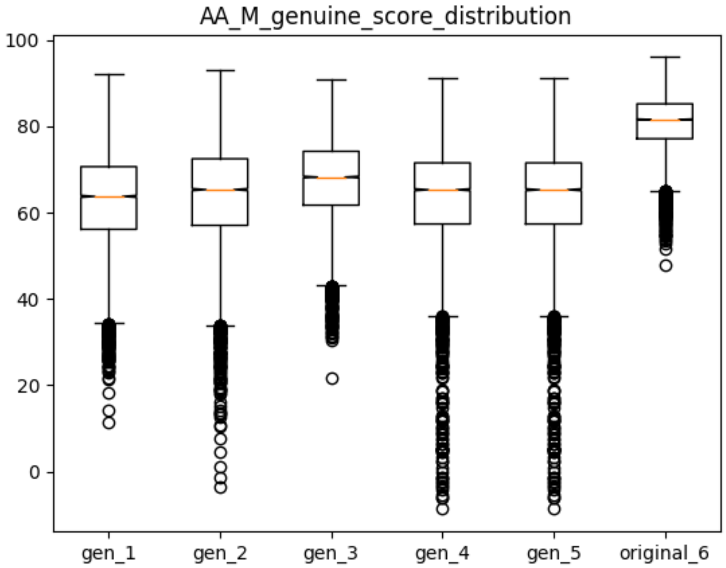

Figure 5.21: Box Plot for AA_M Genuine Intra Subject

- (subject1Image1_original6, subject1Image3_gen2)
- (subject1Image2_original6, subject1Image1_gen2)
- (subject1Image2_original6, subject1Image3_gen2)
- (subject1Image3_original6, subject1Image1_gen2)
- (subject1Image3_original6, subject1Image2_gen2)

The score generated from each intra-subject comparison combination is represented in “gen_2” of the X-axis label.

A high scoring morph subject with intra-subject genuine comparison is shown in 5.23. The scores in this figure consistently high, on the other hand, we can see a

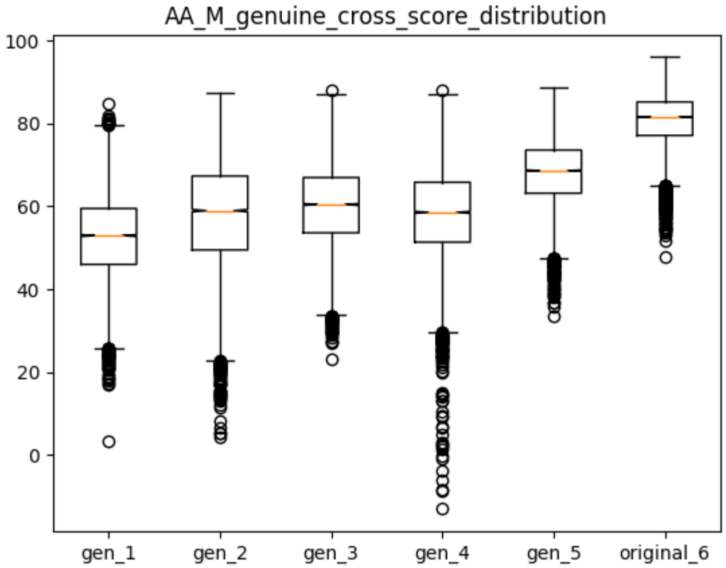

Figure 5.22: Box Plot for AA_M Genuine Cross Intra Subject

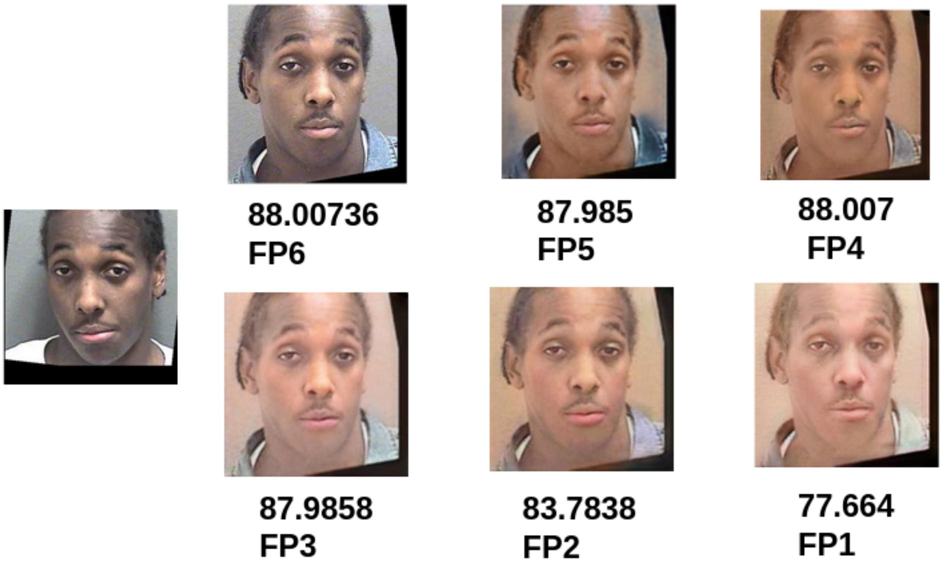

Figure 5.23: High scoring sample

gradual drop in the score when the color of the skin is manipulated with different class types.

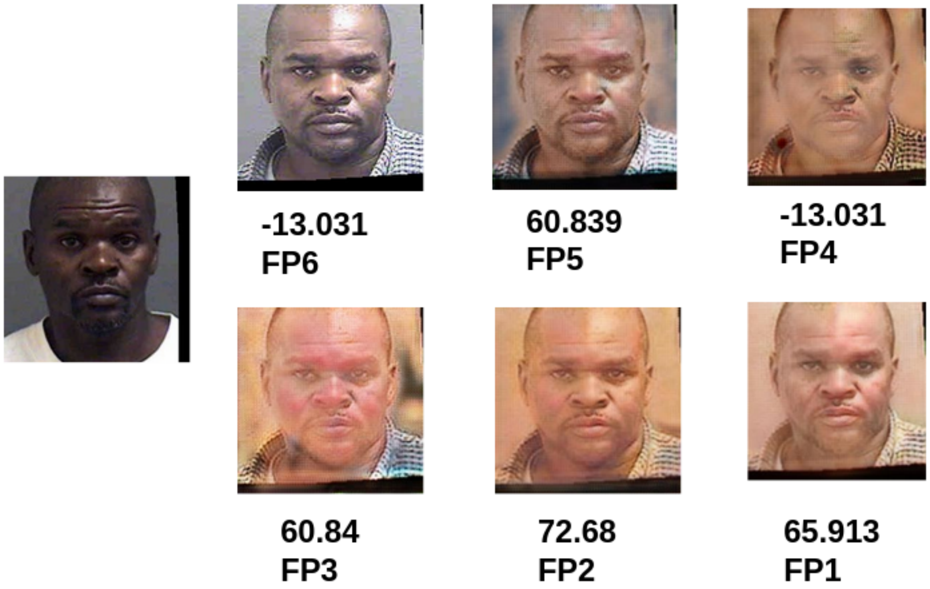

Figure 5.24: Low scoring sample

The low scoring subject in figure 5.24 is a special case scenario where we can see the original to original comparison has a low score of -13.03 whereas the images subsequently generated using our approach tend to have a high score. The faulty images with a constant increase and decrease in scores have to be further investigated to come up with certain conclusions.

The generated images and figures thus gives us an indication of skin affecting the facial recognition system, but drawing any concrete statement requires improvement in the training dataset, isolating female and male subjects, increasing the images per Fitzpatrick class, and other hyper-parameter tunning on the training sets.

Chapter 6

Conclusion

Analyzing the plots and scores generated by our experimental approach we come to the conclusion that altering the skin color of an individual by preserving identity has a significant impact on the facial recognition algorithm. However, the impact seems to be persistent in either direction, whether a darker skin is changed to light or vice versa. As GANs are subject to introduction noise at each training epochs any conclusive statement can not be inferred about skin tone being the only driving for FRAs. Other facial factors like the presence of makeup in the female subject and facial hairs in male sunset can induce the effects on the testing set. However, due to the consistency in low scores and high scores of the intra-subject comparison can of the original and generated dataset, we can conclude that GANs can be used to alter the skin color of an image without affecting the facial features.

Future Work

The experimental approach and literature review highlights the lack of a proper skin tone color classification system defined in cohesion with dermatologists. The upper and lower bound for the classification system can be inferred by applying a k-mean clustering algorithm with six cluster centers to better understand the separation of each skin type class. Our experiment did not focus on generates the intermediate training models as it only converts Type I and Type 6 images. Training and model generation for FP-2 to FP-5 should be conducted for a better understanding of the impact of skin tone. The training set can be improved by increasing the number of images in each Fitzpatrick Types and conduction training as well as testing on the female and male subset separately.

Bibliography

[1] Diana Borza, Adrian Sergiu Darabant, and Radu Danescu. “Automatic Skin Tone Extraction for Visagism Applications.” In: *VISIGRAPP (4: VISAPP)*. 2018, pp. 466–473.

[2] Joy Buolamwini and Timnit Gebru. “Gender shades: Intersectional accuracy disparities in commercial gender classification”. In: *Conference on fairness, accountability and transparency*. 2018, pp. 77–91.

[3] Jiankang Deng et al. “Arcface: Additive angular margin loss for deep face recognition”. In: *Proceedings of the IEEE Conference on Computer Vision and Pattern Recognition*. 2019, pp. 4690–4699.

[4] Jiankang Deng et al. “Lightweight face recognition challenge”. In: *Proceedings of the IEEE International Conference on Computer Vision Workshops*. 2019, pp. 0–0.

[5] Michael Galarnyk. *Understanding Boxplots*. `https://towardsdatascience.com/understanding-boxplots-5e2df7bcbd51`. July 2020.

[6] P. Grother, M. Ngan, and K. Hanaoka. *NISTIR 8280: Ongoing Face Recognition Vendor Test (FRVT) Part 3: Demographic Effects*. `https://nvlpubs.nist.gov/nistpubs/ir/2019/NIST.IR.8280.pdf`.

[7] Souhail Guennouni, Anass Mansouri, and Ali Ahaitouf. *Biometric Systems and Their Applications*. https://www.intechopen.com/online-first/biometric-systems-and-their-applications. Mar. 2019.

[8] Dongyoon Han, Jiwhan Kim, and Junmo Kim. "Deep Pyramidal Residual Networks". In: *Proceedings of the IEEE Conference on Computer Vision and Pattern Recognition (CVPR)*. July 2017.

[9] Kaiming He et al. "Deep Residual Learning for Image Recognition". In: *Proceedings of the IEEE Conference on Computer Vision and Pattern Recognition (CVPR)*. June 2016.

[10] Anil K Jain, Arun A Ross, and Karthik Nandakumar. *Introduction to biometrics*. Springer Science & Business Media, 2011.

[11] 2019 Jocelyn KaiserNov. 7 et al. *A judge said police can search the DNA of 1 million Americans without their consent. What's next?* https://www.sciencemag.org/news/2019/11/judge-said-police-can-search-dna-millions-americans-without-their-consent-what-s-next. Nov. 2019.

[12] Tero Karras, Samuli Laine, and Timo Aila. "A Style-Based Generator Architecture for Generative Adversarial Networks". In: *The IEEE Conference on Computer Vision and Pattern Recognition (CVPR)*. June 2019.

[13] Brendan Klare. *Race and Face Recognition Accuracy: Common Misconceptions*. https://blog.rankone.io/2019/09/12/race-and-face-recognition-accuracy-common-misconceptions/. Dec. 2019.

[14] Sarvasv Kulpati. *A Brief Introduction To GANs (and how to code them)*. https://medium.com/sigmoid/a-brief-introduction-to-gans-and-how-to-code-them-2620ee465c30. May 2019.

[15] Chien Le and R Jain. "A survey of biometrics security systems". In: *EEUU. Washington University in St. Louis* (2009).

[16] Abigail Klein Leichman. *6 futuristic Israeli biometric techs that will transform our lives*. https://www.israel21c.org/6-futuristic-israeli-biometric-techs-that-will-transform-our-lives/. Oct. 2016.

[17] Tingting Li et al. "Beautygan: Instance-level facial makeup transfer with deep generative adversarial network". In: *Proceedings of the 26th ACM international conference on Multimedia*. 2018, pp. 645–653.

[18] Brianna Maze et al. "Iarpa janus benchmark-c: Face dataset and protocol". In: *2018 International Conference on Biometrics (ICB)*. IEEE. 2018, pp. 158–165.

[19] Vidya Muthukumar et al. "Understanding Unequal Gender Classification Accuracy from Face Images". In: *ArXiv* abs/1812.00099 (2018).

[20] S. Pankanti, R. M. Bolle, and A. Jain. "Biometrics: The future of identification [Guest Eeditors' Introduction]". In: *Computer* 33.2 (2000), pp. 46–49.

[21] Krishnapriya K. S et al. "Characterizing the Variability in Face Recognition Accuracy Relative to Race". In: *Proceedings of the IEEE/CVF Conference on Computer Vision and Pattern Recognition (CVPR) Workshops*. June 2019.

[22] Silonie Sachdeva et al. "Fitzpatrick skin typing: Applications in dermatology". In: *Indian Journal of Dermatology, Venereology, and Leprology* 75.1 (2009), p. 93.

[23] Shahnewaz. *Multimodal biometric System for human identification*. https://www.m2sys.com/blog/important-biometric-terms-to-know/the-advantages-of-multimodal-biometric-system-for-human-identification/. Jan. 2019.

[24] Lavanya Shukla. *Fundamentals of Neural Networks on Weights & Biases*. https://www.wandb.com/articles/fundamentals-of-neural-networks/ . Aug. 2019.

[25] Skorzewiak. *Hands typing on laptop keyboard with watching eye on hologram screen.* https://www.shutterstock.com/image-photo/hands-typing-on-laptop-keyboard-watching-1361794664.

[26] Aleksandr Solonskyi. *Why you should use multimodal biometric verification for security systems*. https://towardsdatascience.com/why-you-should-use-multimodal-biometric-verification-for-security-systems-f345134ffd05 . Apr. 2020.

[27] Dr. Meka James Stephen and P.V.G.D. Reddy. "Implementation of Easy Fingerprint Image Authentication with Traditional Euclidean and Singular Value Decomposition Algorithms". In: *International Journal of Advances in Soft Computing and Its Applications* Vol. 3 (July 2011), pp. 1–19.

[28] Jiande SUn, Yufei Wang, and Jing Li. *Gait Recognition*. https://www.intechopen.com/books/motion-tracking-and-gesture-recognition/gait-recognition. July 2017.

[29] Danny Thakkar. *Retinal vs. Iris Recognition: Your Eyes Can Get You Identified?* https://www.bayometric.com/retinal-vs-iris-recognition/. Aug. 2018.

[30] John Trader. *The Top 5 Uses of Biometrics Applications across the Globe*. https://www.m2sys.com/blog/biometric-hardware/top-5-uses-biometrics-across-globe/. June 2020.

[31] Kambiz Youabian. *Dermatone skin analyzer*. US Patent App. 11/183,572. Jan. 2007.

[32] Seyma Yucer et al. "Exploring Racial Bias within Face Recognition via per-subject Adversarially-Enabled Data Augmentation". In: *Proceedings of the IEEE/CVF Conference on Computer Vision and Pattern Recognition Workshops*. 2020, pp. 18–19.

[33] Jun-Yan Zhu et al. "Unpaired Image-To-Image Translation Using Cycle-Consistent Adversarial Networks". In: *The IEEE International Conference on Computer Vision (ICCV)*. Oct. 2017.